Chapter 2
Nanoporous Copper Metal Catalyst in Click Chemistry: Nanoporosity Dependent Activity Without Supports and Bases

Abstract Nanoporous copper catalysts with tunable nanoporosity were fabricated from $Cu_{30}Mn_{70}$ alloy by controlling the dealloying temperature under free corrosion conditions. The tunable nanoporosity of CuNPore led to a significant enhancement of catalytic activity in click chemistry without using any supports and bases. Characterization of CuNPore surface, high reusability, leaching experiment, and formation of nanostructured copper acetylide revealed that the click reaction occurred at the catalyst surface and the Cu(I) species was the real catalytic active sites. The CuNPore catalyst system was also applied to the three-component coupling of terminal alkynes, tosyl azide and dialkylamines to afford the corresponding aminoimines in high yields.

Keywords Click chemistry · Nanoporous copper catalyst · Heterogeneous catalysis · High reusability

2.1 Introduction

Nanoporous metals are promising materials for catalysis [1–9], sensing [10–12], and actuation [13, 14] applications due to their interesting structural, optical and surface properties. In spite of the growing number of studies on various applications of nanoporous metals, the catalytic properties in chemical reactions are still less explored, although the interesting features of nanoporous metals make them potentially attractive candidates for new heterogeneous catalysts [1–9]; the three-dimensional open-pore network structures and metal ligaments allow the transport of molecules and ions, a high surface-to-volume ratio in comparison with bulk metals results in outstanding catalytic efficiency; furthermore, the potentially high reusability and rather simple work-up are favorable for practical synthetic methodology. Moreover, in contrast to the supported nanoparticles (NPs) catalyst, a nanoporous metal without supports should be a challenging catalyst system to understand the relevant catalytic mechanism more easily and to extend the catalytic application widely by elimination of the support effect problems and

M. Yan, *Development of New Catalytic Performance of Nanoporous Metals for Organic Reactions*, Springer Theses, DOI: 10.1007/978-4-431-54931-4_2,

relaxation of aggregation. In this regard, we have focused on the study of the catalytic properties of unsupported nanoporous metals in organic molecular transformations under liquid phase conditions [15, 16]. Nanoporous gold exhibited a remarkable catalytic efficiency and reusability in the oxidation of organosilanes into silanoles with water [15], and non-porous palladium without ligands and supports showed high catalytic activity and reusability in the Suzuki coupling [16]. Therefore, the design and synthesis of new and efficient nanoporous metal catalytic systems for development of molecular transformations are highly desirable.

In 2002, Sharpless [17] and Meldal [18] reported independently the Huisgen [3 + 2] cycloaddition of terminal alkynes and organic azides catalyzed by homogeneous Cu(I) salts, the so-called click reaction. This methodology has been emerged as the most powerful tool for connecting the two useful functional groups. During the last few years, numerous applications of the click reaction have been reported in the field of material sciences, bio- and medicinal chemistry [19–21]. The click reaction can be catalyzed also by heterogeneous copper(I), such as immobilized copper nanoclusters and copper/cuprous oxide NPs, copper-in-charcoal NPs, copper zeolites, and copper nitride NPs supported on mesoporous SiO_2 with or without bases [22–30]. Copper metal alone also has been reported to catalyze this click reaction, while the reaction is relatively slow and requires high catalyst loading [31]. Recyclability of these heterogeneous copper catalysts was rarely reported [30]. Recently, it has been reported that the monolithic CuNPore is a promising high strength/low density material, which can be synthesized through the chemical or electrochemical de-alloying of various single-phase Cu/M (M = Al, Mg, Mn) alloys [32–36]. Herein, we report an efficient approach for the synthesis of CuNPore with tunable nanoporosity and its remarkable catalytic properties in click chemistry without using any supports and bases (Eq. 2.1). To the best of our knowledge, this is the first report on a monolithic CuNPore-catalyzed molecular transformation, while the non-monolithic CuNPore in the form of Raney copper is a well known catalyst in the water-gas shift reaction [37, 38].

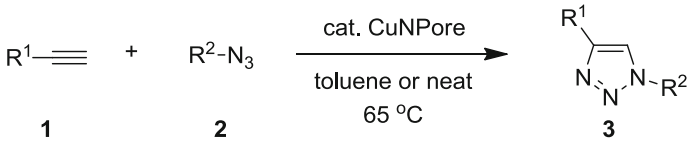

(2.1)

2.2 Results and Discussion

2.2.1 Synthesis of Nanoporous Copper

Nanoporous metals with ideal bicontinuous structures can be synthesized by chemical or electrochemical dealloying of binary or ternaryl alloys by selective dissolution of one or more of the components of the alloy. To obtain uniform

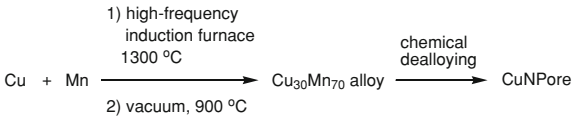

Scheme 2.1 Synthesis of $Cu_{30}Mn_{70}$ alloy and CuNPore by chemical dealloying

nanoporosity upon dealloying, an alloy system is usually required to be in monolithic phase because the nanoporosity is formed by a self-assembly process through surface diffusion, not by the simple excavation of one phase from a preseparated multiphase system. Surface diffusion of the less reactive component across the alloy/solution interface plays a key role in the formation of nanoporous metals and has a significant influence on size of ligament/pore. Furthermore, the electrochemical activities of elements in an alloy may be significantly different from the environment, which can strongly affect dissolution process and dealloying morphology; this relationship indicates that the compositions of starting alloys also have a significant influence on the nanostructure of porous metals.

CuNPore is a promising, high strength/low density material, because of its high porosity and yield strength of 86 ± 10 MPa. Recently, it has been reported that monolithic CuNPores can be synthesized through the chemical or electrochemical dealloying of various Cu/M (M = Al, Mg, Mn, etc.) alloys [32–36]. Hayes et al. [32] and Chen et al. [36] reported the synthesis of monolithic CuNPores by chemical/electrochemical dealloying of a single-phase $Cu_{30}Mn_{70}$ alloy under acidic conditions with ligaments of length 10–125 nm. Zhang et al. have also synthesized monolithic CuNPores with a ligament length of several hundred nanometers from dual-phase Cu/Al and Cu/Mg alloys by chemical dealloying in HCl solution [33, 34]. Most recently, Liu et al. succeeded in synthesis of CuNPres with ligament lengths from 20–200 nm through chemical dealloying in an alkaline solution by altering the Cu/Al ratio of the initial alloys [45, 46]. In view of the industrial applications of these products, widespread use of the dealloying technique to make CuNPores is frequently hindered by the high cost of such unreactive metals and by the limited range of alloy systems. To date, little attention has been paid to the synthesis of CuNPores with tunable nanoporosity by means of changing the dealloying conditions; although it has been proved that materials with smaller nanostructure will offer higher surface area, which may significantly enhance catalytic properties. The Cu alloy that best fits these requirements is $Cu_{30}Mn_{70}$. Recently, Chen et al. obtained CuNPores with tunable nanopore sizes from Cu/Mn ribbons by controlling chemical dealloying time in a diluted HCl solution [36]. However, the small dimensions (thickness $\approx$20 μm; width $\approx$1 mm) of the ribbon used would cause it to be brittle during the catalytic transformations. Investigation of the synthesis of CuNPore catalysts with suitable dimensions and smaller pore/ligament size is highly desirable.

The alloy $Cu_{30}Mn_{70}$ was synthesized from pure Cu (99.99 wt%) and Mn (99.99 wt%) at 1300 °C in a high-frequency induction furnace. The Cu/Mn alloy, sealed in quartz tube under vacuum, was heated at 900 °C for 72 h and then

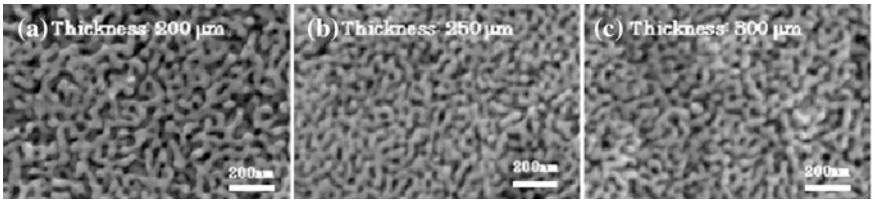

Fig. 2.1 SEM images of CuNPore synthesized by dealloying of $Cu_{30}Mn_{70}$ in 1 $_M$ $(NH_4)_2SO_4$ and 0.01 $_M$ $MnSO_4$ at 25 °C from rolled alloys with thicknesses of **a** 200 μm (cat-1), **b** 250 μm (cat-2), **c** 300 μm (cat-3)

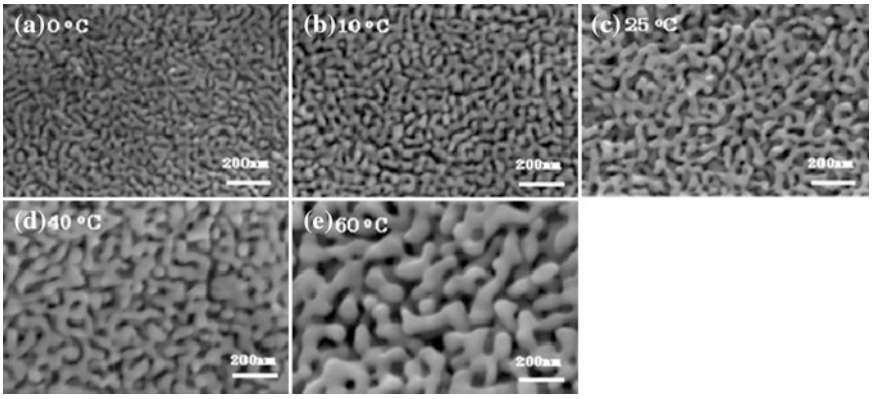

Fig. 2.2 SEM images of CuNPore synthesized by dealloying of $Cu_{30}Mn_{70}$ (200 μm thickness) in 1 $_M$ $(NH_4)_2SO_4$ and 0.01 $_M$ $MnSO_4$ at **a** 0 °C (cat-4), **b** 10 °C (cat-5), **c** 25 °C (cat-1), **d** 40 °C (cat-6), **e** 60 °C (cat-7)

quenched into water (Scheme 2.1). The resulting alloy was sectioned using a diamond saw into samples approximately 1 mm in thickness. The samples were rolled into films of thicknesses of about 200, 250, and 300 μm for dealloying.

Various CuNPores with versatile ligament scales and morphologies were synthesized by chemical dealloying with two kinds of electrolytes following Hayes' method [32] 5 × 5 mm pieces of the three thickness of rolled $Cu_{30}Mn_{70}$ were placed directly in pre-prepared electrolyte 1 $_M$ $(NH_4)_2SO_4$ and 0.01 $_M$ $MnSO_4$ at room temperature for 6 days. SEM imaging (Fig. 2.1) showed that ligament and nanopore channels were formed uniformly. The average ligament diameters were estimated as ≈40 nm for the 200 μm thickness alloy (cat-1), ≈35 nm for both the 250 and 300 μm thickness alloys (cat-2 and cat-3). EDX analysis showed that the residual Mn composition of CuNPores remains approximately constant at 1–2 at. %. In the same electrolytes, the rolled $Cu_{30}Mn_{70}$ alloy with a thickness of ≈200 μm was treated at different temperatures, producing CuNPores with a tunable diameter; ≈25 nm at 0 °C (cat-4), ≈30 nm at 10 °C (cat-5), ≈50 nm at 40 °C (cat-6), ≈70 nm at 60 °C (cat-7) (Fig. 2.2). EDX analysis showed that the residual Mn composition of the 0 °C dealloyed sample (cat-4) is ≈4 at. %, and

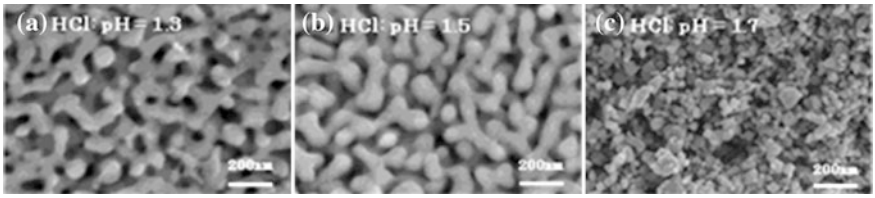

Fig. 2.3 SEM images of CuNPore fabricated by dealloying of $Cu_{30}Mn_{70}$ (200 μm thickness) in HCl solution with pH **a** 1.3 (cat-8), **b** 1.5 (cat-9), **c** 1.7 (cat-10)

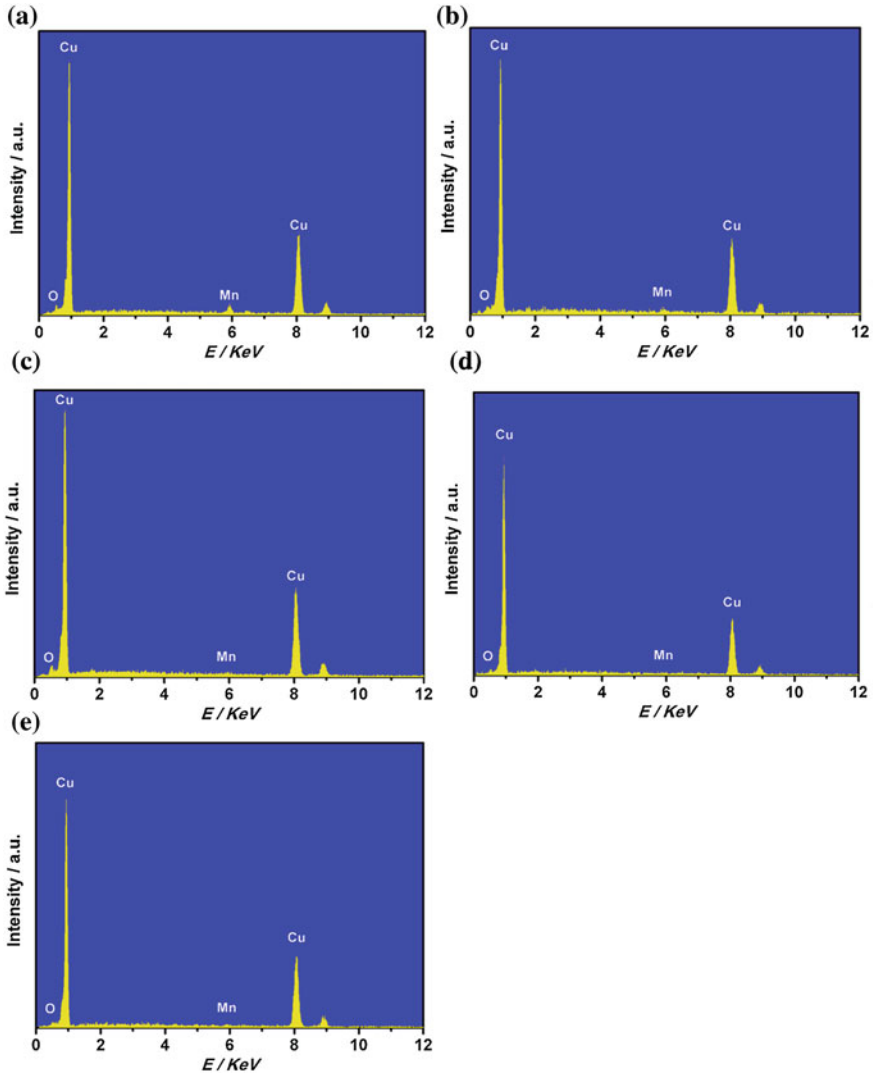

Fig. 2.4 EDX spectra of **a** cat-4 made at 0 °C, $Cu_{96}Mn_4$,**b** cat-5 made at 10 °C, $Cu_{98}Mn_2$, **c** cat-1 made at 25 °C, $Cu_{98}Mn_2$, **d** cat-6 made at 40 °C, $Cu_{98}Mn_2$, **e** cat-7 made at 60 °C, $Cu_{98}Mn_2$

Table 2.1 Influence of ligament size and initial alloys on CuNPore catalytic activity in the CuAAC reaction

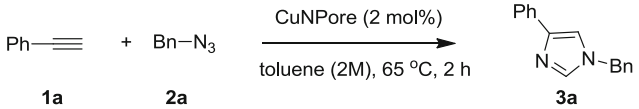

1a **2a** **3a**

Entry	CuNpore catalyst	Ligament size, nm	Alloy thickness, μm	Electrolyte[a]	Yield 3a, [b] (%)
1	cat-1	40	200	A (25 °C)	99[c]
2	cat-2	35	250	A	83
3	cat-3	35	300	A	40
4	cat-4	25	200	A (0 °C)	42
5	cat-5	35	200	A (10 °C)	51
6	cat-6	50	200	A (40 °C)	69
7	cat-7	70	200	A (60 °C)	48
8	cat-8	60	200	B (Ph 1.3)	85
9	cat-9	70	200	B (pH 1.5)	60
10	cat-10	–	200	B (pH 1.7)	69
11	$Cu_{30}Mn_{70}$	–	200	–	0
12	Cu_2O	–	–	–	3
13	CuO	–	–	–	3

The reaction of phenylacetylene and benzyl azide was carried out in the presence of 2 mol% of Cu catalyst in toluene at 65 °C, for 2 h

[a] A: 1 $_M$ $(NH_4)_2SO_4$ and 0.01 $_M$ $MnSO_4$; B: HCl solution

[b] ^{1}H NMR yield determined using CH_2Br_2 as an internal standard

[c] Isolated yield

remains approximately constant at ≈2 at. % for cat-5 to cat-7 (Fig. 2.4). Dealloying of the 200 μm thickness $Cu_{30}Mn_{70}$ alloy in HCl solution resulted in large ligaments with an average diameter of 60–70 nm (Fig. 2.3a, b, cat-8 and cat-9); in the reduced concentration, a non-nanopore structure was observed (Fig. 2.3c, cat-10). These results indicate that the dealloying conditions and the nature of initial alloys significantly influence the nanopore/ligament size and morphology in dealloyed CuNPores.

2.2.2 The Influence of CuNPore Structures on Catalytic Activity in the 1,3-dipolar Cycloaddition of Terminal Alkynes and Organic Azides

Various CuNPore materials were used as catalysts in the CuAAC reaction of phenylacetylene and benzyl azide in toluene at 65 °C for 2 h and the influence on catalytic activity of their ligament sizes and morphology was examined (Table 2.1). CuNPore catalysts synthesized from alloys of different thickness were also tested; cat-1 showed the highest activity (entries 1–3). Of the CuNPore

Table 2.2 CuNPore (cat-1)-catalyzed synthesis of various substituted triazoles

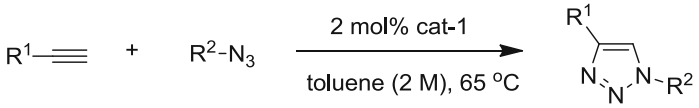

1 **2** **3**

Entry	R^1 1	R^2 2	Time, h	Yield, (%)[a]
1	2-pyridyl 1b	Bn 2a	4.5	3b, 96
2	3-thienyl 1c	Bn 2a	7	3c, 99
3	n-pentyl 1d	Bn 2a	6	3d, 99
4	c-hexyl 1e	Bn 2a	4	3e, 97
5	t-Bu 1f	Bn 2a	22	3f, 99
6	$HOCH_2$ 1g	Bn 2a	19	3 g, 94
7[b]	Ph 1a	Ph 2b	22	3 h, 95
8[b]	Ph 1a	Cinnamyl 2c	19	3i, 99
9	Ph 1a	EtO_2CCH_2 2d	3	3j, 99
10	$BnNHCH_2$ 1h	Ph 2b	3.5	3k, 95
11[c]	$TsNHCH_2$ 1i	Ph 2b	6	3l, 98

To a toluene (2 M) solution of cat-1 (2 mol%) was added alkyne **1** and azide **2** (1 equiv.). The mixture was stirred at 65 °C for the time shown in the table

[a] Isolated yield

[b] 2 equiv. azide were used

[c] 1.2 equiv. azide were used

catalysts with controlled ligament sizes, cat-1, with a ligament size of about 40 nm, showed the greatest activity, affording the corresponding 1,2,3-triazoles in almost quantative yield (entry 1 vs. entries 4–7). It is well known that nanocatalysts of smaller sizes exhibit greater catalytic activity as a result of their high surface areas; however, these results were unprecedented. The specific surface area of cat-3 was measured by the BET method to be 14 m^2/g, the turnover frequency (TOF) thus reached to 0.26 s^{-1}. It should be noticed that the reaction can be catalyzed by cat-3 at ambient temperature, although it required a longer reaction time (30 h). Cu-Mn alloy was totally inactive as a catalyst (entry 11). These results indicate that the tunable nanoporosity of CuNPore has a strong influence on catalytic activity in the click reaction, however the reason for this remains unresolved. Further examination of the dealloyed Cu catalysts synthesized in HCl solution (cat-8–10), revealed them to be less active (entries 8–10).

The catalytic activity of CuNPore (cat-1, 2 mol%) was further examined with various terminal alkynes and organic azides in toluene (2 M) at 65 °C (Table 2.2). Not only aromatic and heteroaromatic alkynes but also alkylalkynes were catalyzed regioselectively, affording 1,2,3-triazoles in excellent yields (entries 1–7). Various functional groups, such as alkene, ester, and protected amines were tolerated under the present heterogeneous conditions (entries 8–11). Under neat conditions, the catalytic loading can be decreased to 0.1 mol% without any significant influence on the reaction efficiency, and the TOF was increased up to 5.2 s^{-1} (Eq. 2.2).

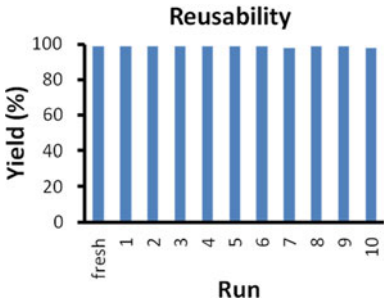

Fig. 2.5 Reusability of CuNPore (cat-1) for the reaction of **1a** with **2a** was carried out in toluene (0.5 M) at 65 °C for 6 h

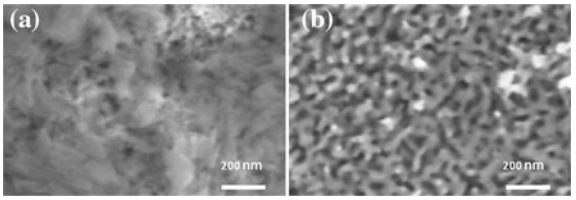

Fig. 2.6 SEM images of cat-1 after tenth cycle. **a** Surface was not clear, **b** Cross-sectional nanostructure remained well

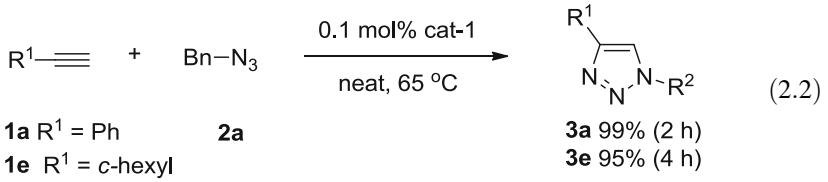

(2.2)

The CuNPore (cat-1) catalyst was reused for multiple cycles without significant loss of catalytic activity in the reaction of **1a** and **2a**; the yield was still 98 % in the tenth cycle (Fig. 2.5). After simple filtration of the reaction mixture, the catalyst was washed with acetone and reused without further purification. The product was produced almost quantitatively in every cycle and the turnover number (TON) reached up to 8200. It is noteworthy that the nanostructure of the recovered catalyst did not show significant changes after the fifth cycle, however, the nanostructure on surface was not clear after the tenth cycle while the cross-sectional nanostructure survived well (Fig. 2.6).

The CuNPore catalyst system can be further applied to the three-component coupling of terminal alkynes, tosyl azide and dialkylamines to afford the corresponding aminoimines in high yields; this was previously reported for homogeneous Cu catalysts (Scheme 2.2) [47]. The reactions tolerated different functional groups and the catalyst could be reused at least once without loss of catalytic activity. In addition, the three-component coupling gave an excellent yield, whereas the reaction over the reported homogeneous Cu catalyst afforded a mixture of products. This result implies that CuNPore catalysts can be applied to a range of other transformations with high activity and selectivity.

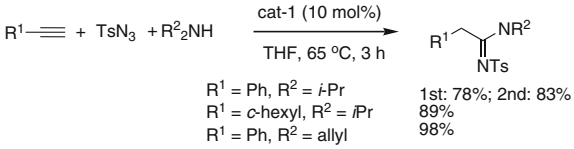

Scheme 2.2 Application of a CuNPore catalyst to the three-component coupling of terminal alkynes, tosyl azide, and dialkylamines

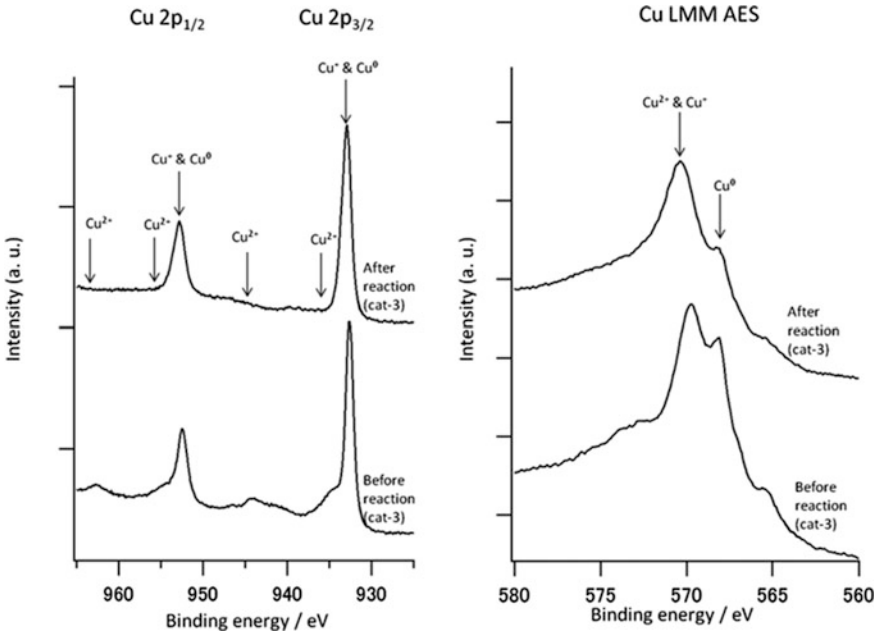

Fig. 2.7 XPS spectra of CuNPore catalyst (cat-1) surface before reaction and after reaction

2.2.3 Mechanistic Investigation

A number of homogeneous and heterogeneous examples proved that the click reaction was catalyzed by Cu(I) species [17–30]. X-ray photoelectron spectroscopy (XPS) spectra showed that the fresh CuNPore (cat-1) surface is composed of Cu(0), Cu(I), and Cu(II) species, while Cu(I) is a predominant component (Fig. 2.7) [41]. The Cu 2*p* peaks at 932 and 953 eV and Cu LMM Auger peak at 568 eV were assigned to Cu(0); peaks at 570, 932, and 953 eV were ascribed to Cu(I); several satellite peaks at 935 eV, 944 eV, 955 eV, and 963 eV correspond to Cu(II). The Cu(I) and Cu(II) ions exist as the native Cu_2O and CuO on CuNPore surface. The XPS spectra of cat-1, cat-4 to cat-7 having different ligament sizes did not show a significant difference on the surface component (Fig. 2.8). Moreover, after reaction, the satellite peaks of Cu(II) were almost disappeared while Cu(I)

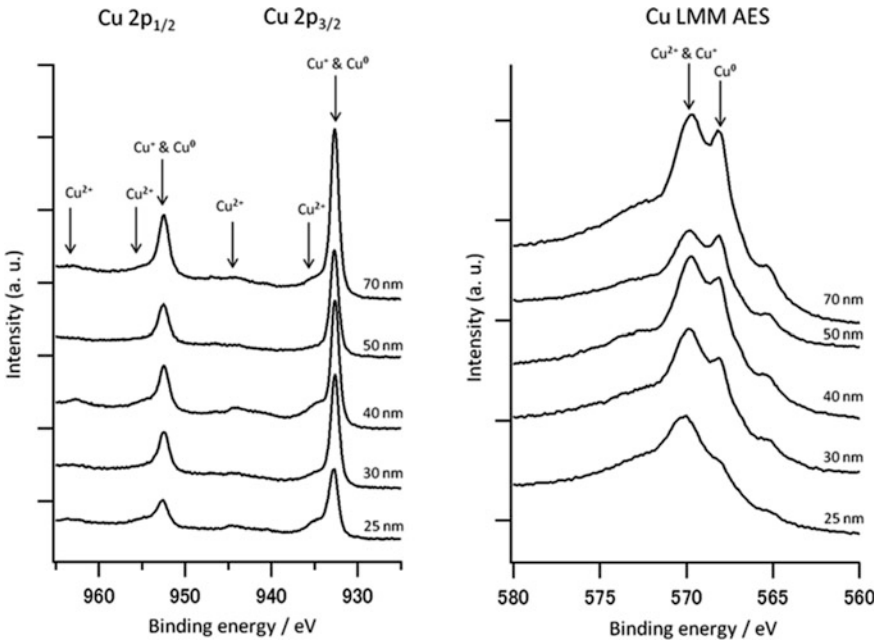

Fig. 2.8 XPS spectra of CuNPore materials with different ligament sizes

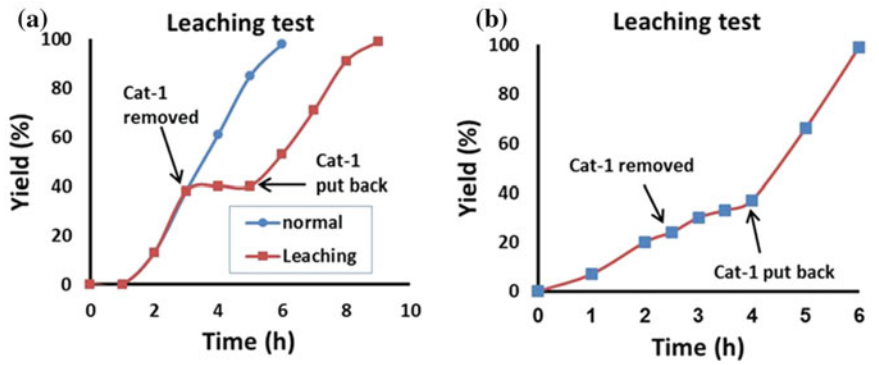

Fig. 2.9 Leaching test of CuNPore for the reaction of phenylacetylene and benzylazide with cat-1 at 65 °C **a** in toluene, **b** in THF

remained predominantly (Fig. 2.7). This result suggested that some amounts of Cu metal might be leached to the organic solvent. Indeed, the inductively coupled plasma (ICP-AES) analysis showed that only 0.2 ppm of Cu was leached after reaction. To clarify whether the leached Cu metal catalyzes the present reaction or not, we monitored the reaction with or without catalyst. The reaction of **1a** and **2a** was carried out by using 5 mol% of cat-1 in toluene (0.5 M) at 65 °C. After 3 h, CuNPore catalyst was removed from the reaction vessel and **3a** was produced in

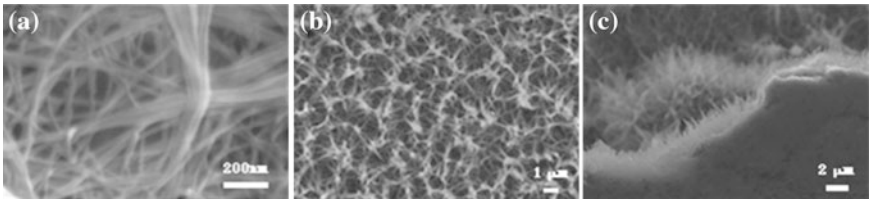

Fig. 2.10 SEM images of nanostructured copper acetylide **a** grass-like material on surface, **b** magnified surface, **c** cross sectional structure image

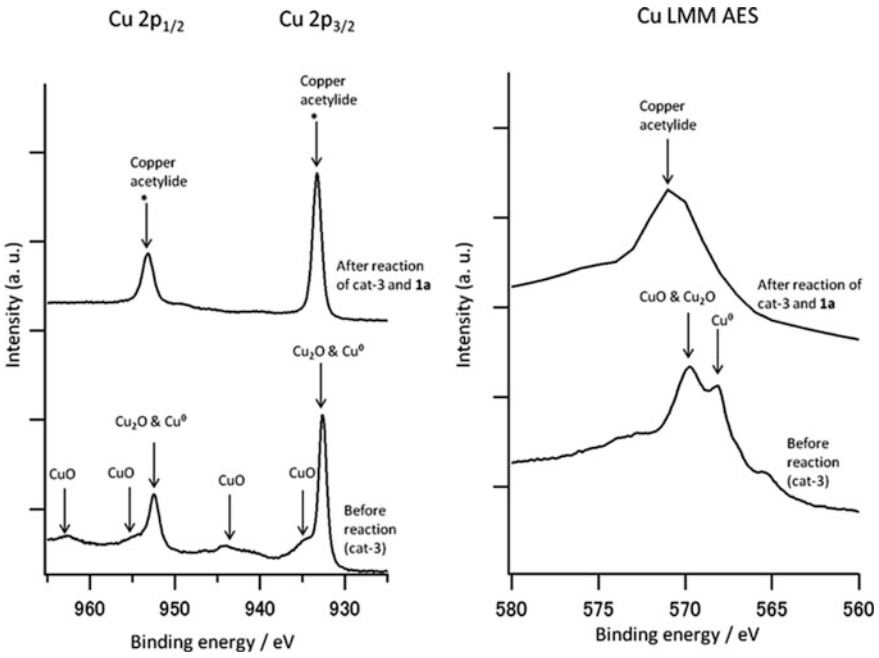

Fig. 2.11 XPS spectra of nanostructured copper acetylide

38 % ^{1}H NMR yield at this time (Fig. 2.9a, ■ symbols). The reaction mixture was continuously heated in the absence of the catalyst for 1 h, affording **3a** in 40 % yield, while the reaction was completely stopped in the next 1 h. The reaction restarted when cat-1 was put back into the mixture and finally gave **3a** in 99 % yield within 4 h. On the other hand, the control reaction without removal of catalyst was complete in 6 h, giving **3a** in 98 % yield (Fig. 2.9a, ● symbols). These results indicated that the leached copper was mainly Cu(II) species which was unable to catalyze the present click reaction, suggesting that the reaction is catalyzed by Cu(I) ions on the CuNPore surface. It should be noted that Cu_2O or CuO powder cannot catalyze this reaction without a base (Table 2.1, entries 12 and 13). These results further support that the nanoporous structure plays a crucial

role in the current catalysis. In contrast, when THF was used as solvent instead of toluene in the same control reaction, the reaction slowed down after removal the catalyst, but did not stop, implying that leached Cu^{I} species are stabilized by THF preventing easy oxidization to Cu^{II} (Fig. 2.9b). ICP analysis showed that only a negligible amounts of Cu were leached in the reaction in toluene and THF, 0.2 and 0.11 ppm, respectively.

Involvement of copper(I) acetylide species in the click reaction is well demonstrated by computational study and kinetic experiments [42–44]. During this study of the catalytic properties of CuNPore materials, we found that when cat-1 was treated with an excess amount of phenylacetylene in toluene without organic azides at room temperature, the CuNPore catalyst surface was turned to yellow after washing with acetone and dichloromethane. The SEM image showed that cat-1 surface was covered with a uniform grass-like material (Fig. 2.10). A binding energy peak appeared in between those of CuO and Cu_2O, and peaks of Cu(II) and Cu(0) were not detected in the XPS spectra, suggesting that the new peaks (marked by *) of the grass-like material surface should be assigned to Cu(I) species (Fig. 2.11). However, treatment of cat-1 with benzyl azide without phenylacetylene did not change the nanoporous structure of the catalyst. These results prompted us to examine the possibility of the nanostructured copper acetylide formation. When the grass-like material (Fig. 2.10) was treated with benzyl azide at 65 °C for 2 h, the grass-like material disappeared from the surface, and the nanoporous structure of cat-1 was recovered, and a very small amount of the corresponding triazole **3a** was detected by ^{1}H NMR and GC-MS. Moreover, the recovered CuNPore remained its high catalytic activity in the reaction of **1a** and **2a** (99 % of **3a**), although the reaction with the grass-like material as a catalyst gave 58 % of **3a**. These results implied that the grass-like material should be the nanostructured *polymeric* copper acetylide which was less active than the copper acetylides with lower order aggregates generated in situ. The results were in good agreement with the previous DFT studies and experimental investigation reported by Fokin [42, 43] and Straub [44]. It is noteworthy that the nanostructured copper acetylide was very stable in air compared to the air-sensitive fresh CuNPore, suggesting that the polymeric copper acetylide can be used as a CuNPore metal storage to protect the nanoporosity of CuNPore from air.

2.3 Conclusion

we have developed an efficient approach for the fabrication of nanoporous copper materials with tunable nanoporosity, and demonstrated that CuNPore has an outstanding catalytic activity for the click chemistry without using any supports and bases. The catalytic activity was highly in dependence on the ligament (or pore) sizes of the CuNPore materials; ligament size about $\sim$40 nm significantly enhanced the catalytic efficiency. Characterization of the catalyst surface, leaching experiments, and the formation of nanostructured copper acetylide revealed that

the present click reaction is catalyzed by Cu(I) species on the CuNPore surface. The CuNPore catalyst exhibited a high reusability; it can be recycled for ten times without significant loss of activity. A wide range of alkynes and azides can be tolerated, giving the corresponding triazoles in excellent yields. The CuNPore catalyst system can also be applied to the three-component coupling of terminal alkynes, tosyl azide and dialkylamines to afford the corresponding aminoimines in high yields. Further studies on exploring new catalytic activities of CuNPore materials and extension of its utility to organic synthesis are in progress.

2.4 Experimental Section

2.4.1 General Information

^{1}H NMR and ^{13}C NMR spectra were recorded on JEOL JMTC-270/54/SS (JASTEC, 300, 400, 500 MHz) spectrometers. ^{1}H NMR spectra are reported as follows: chemical shift in ppm (δ) relative to the chemical shift of $CDCl_3$ at 7.26 ppm, integration, multiplicities (s = singlet, d = doublet, t = triplet, q = quartet, m = multiplet and br = broadened), and coupling constants (Hz). ^{13}C NMR spectra reported in ppm (δ) relative to the central line of triplet for $CDCl_3$ at 77 ppm. IR spectra were recorded on JASCO FT/IR-4100 spectrometer; absorptions are reported in cm^{-1}. High-resolution mass spectra were obtained on a BRUKER APEXIII spectrometer. The XPS measurements were carried out using a VG ESCALAB 250 spectrometer (Thermo Fisher Scientific K.K.) employing monochromatic Al K X-ray radiation. The system was operated at 15 kV and 200 W. The base pressure of the analysis chamber was less than 10 to 8 Pa. SEM observation was carried out using HITACHI FE-SEM S4300 operated at an accelerating voltage of 10 kV. EDX analysis was carried out using EDAX Genesis with HITACHI FE-SEM S4300 operated at an accelerating voltage of 20 kV. ICP-MS analysis was performed with Shimadzu ICPS-7510. Column chromatography was carried out employing Slica gel 60 N (spherical, neutral, 40 $\sim$ 100 μm, KANTO Chemical Co.). Analytical thin-layer chromatography (TLC) was performed on 0.2 mm precoated plate Kieselgel 60 F_{254} (Merk).

2.4.2 Materials

Anhydrous toluene (WAKO), Cu (99.99 %, MITSUWA), Mn (99.99 %, MITSUWA), alkynes (**1**) and azides (**2**) were purchased and used as received. The structure of products were identified according to the reported literatures [48–52].

2.4.3 Calculation of TOF and TON

The surface area of CuNPore (cat-1, ligament size: ~40 nm) dealloying at room temperature was measured by BET method to be 14 m^2/g, and the density of surface atoms for the energetically most stable Cu(111) surface is 1.77×10^{19} atoms/m^2. The reaction time was 2 h as shown in Table 2.1. Using these values the TOF was calculated to be 936 h^{-1} (Table 2.1, entry 1). On the other hand, TON was calculated to be 8200 by the number of the Cu atoms on the catalyst surface with the number of the product **3a** as shown in Fig. 2.5 [6].

2.4.4 Fabrication of $Cu_{30}Mn_{70}$ Alloy

$Cu_{30}Mn_{70}$ alloys was fabricated from pure Cu (99.99 wt%) and Mn (99.99 wt%) at 1300 °C by high-frequency induction furnace. The Cu–Mn alloy sealed in quartz tube under vacuum was heated at 900 °C for 72 h, and quenched into water [32]. The resulting alloy was sectioned, using a diamond saw, into samples approximately 1 mm thick. The alloy samples were rolled to about 200 μm thickness.

2.4.5 Representative Fabrication Method of Nanoporous Copper (CuNPore, cat-1) Under Free Corrosion

The rolled alloy sample with 200 μm thickness and 5 × 5 mm size was placed directly in 1 M $(NH_4)_2SO_4$ and 0.01 M $MnSO_4$ electrolytes at room temperature (25 °C) for 6 days [32]. All electrolytes were prepared with deionized (DI) water and reagent grade chemicals. After dealloying, the sample was removed from electrolytes and rinsed in DI water for few minutes. The sample was then washed with acetone and dried on vacuum. The dried CuNPore was stored in glove box (Fig. 2.12).

Under same electrolytes, cat-4 and cat-5 were fabricated at 0 and 10 °C for 6 days, respectively. Cat-6 and cat-7 were dealloyed at 40 and 60 °C for 4 days. Cat-2 and cat-3 were fabricated at 25 °C for 6 days.

Under HCl solution, cat-8, cat-9 and cat-10 were fabricated at 25 °C for 6 days.

2.4.6 Representative Procedure for the CuNPore (cat-1)-Catalyzed Click Reaction of Phenyl Acetylene (1a) and Benzyl Azide (2a) (Tables 2.1 and 2.2)

To a toluene (2 M, 0.5 mL) solution of CuNPore (cat-1, 2 mol%, 1.3 mg) was added phenyl acetylene **1a** (1 mmol, 112 μL) and benzyl azide **2a** (1 mmol, 125 μL) in a V-shape reactor vial. The reaction mixture was stirred at 65 °C for 2 h by using a bulky round-shape magnetic stirring bar. After consumption of **1a** and **2a**

Fig. 2.12 CuNPore (cat-3) size: 175 μm (thickness)×5 mm×5 mm

Table 2.3 Reusability of cat-1

Run	Fresh	1	2	3	4	5	6	7	8	9	10
3a, yield (%)[a]	99	99	99	99	99	99	99	98	99	99	98

[a] ^{1}H NMR yield of **3a** determined using dibromomethane as an internal standard

which were monitored by TLC, the reaction mixture was cooled to room temperature. The mixture was filtered and washed with dichloromethane. The recovered CuNPore catalyst was washed with acetone and dried under vacuum. After concentration of the filtrate, the white solid was purified with a short silica gel chromatography, by using a 3:1 mixture of hexane and ethyl acetate as an eluent, to afford 233 mg of 1-benzyl-4-phenyl-1*H*-1,2,3-triazole **3a** (99 %) as a white solid.

2.4.7 Neat Reaction Procedure (Eq. 2.2)

The reaction of **1a** (14.2 mmol, 1.59 mL) and **2a** (14.2 mmol, 1.77 mL) performed using 0.1 mol% of cat-1 (0.9 mg) in the absence of solvent at 65 °C for 2 h. The work-up procedure is same to above. **3a** was obtained in 99 % yield (3.33 g)

2.4.8 Leaching Experiment (Fig. 2.9)

Figure 2.9a, leaching experiment for the reaction of **1a** and **2a** was carried out by using 5 mol% of cat-1 in toluene (0.5 M) at 65 °C. Cat-1 was removed from reaction vial after 3 h, giving **3a** in 38 % NMR yield. The reaction was continuously heated for 1 h in the absence of cat-1, producing **3a** in 40 %. After being heated another 1 h, the yield of **3a** was not changed (40 %). Then, cat-1 was put

back into the reaction mixture and heated for 1 h gave **3a** in 53 % yield. The reaction was finally complete within 3 h produced **3a** in 99 % yield.

On the other hand, under same reaction conditions, the controlled reaction without removal of cat-1 was complete in 6 h, giving **3a** in 98 % yield.

Figure 2.9b, leaching experiment for the reaction of **1a** and **2a** was carried out by using 5 mol% of cat-1 in THF (2 M) at 65 °C. Cat-1 was removed from reaction vial after 2.5 h, giving **3a** in 24 % NMR yield. The reaction was continuously heated for 1.5 h in the absence of cat-1, producing **3a** in 37 %. Then, cat-1 was put back into the reaction mixture and heated for 1 h gave **3a** in 66 % yield. The reaction was finally complete within 1 h produced **3a** in 99 % yield.

2.4.9 Reusability (Fig. 2.5)

The reaction of **1a** and **2a** for the recycle was carried out in toluene (0.5 M) at 65 °C for 6 h in the presence of cat-1 catalyst. After filtration, cat-1 was washed with acetone and dried on vacuum. The recovered cat-1 was continuously used for 10 times. The ^{1}H NMR yield of **3a** for every cycle is shown in Table 2.3.

2.4.10 Formation of Nanostructured Copper Acetylide (Figs. 2.10 and 2.11)

A toluene (2 M, 0.7 mL) solution of cat-1 (2 mol%, 1.7 mg) and phenyl acetylene **1a** (1.34 mmol, 150 μL) was stirred for 3.5 h, the cat-1 surface was turned to yellow (Fig. 2.11). The SEM image showed that the surface was covered with a uniform grass-like material. When the grass-like material was treated with an excess amount of benzyl azide **2a**, the grass-like material was disappeared from SEM image. The nanoporous structure of cat-1 surface was recovered and a small amount of **3a** was observed from ^{1}H NMR and GC-MS. The grass-like material should be the nanostructured copper acetylide.

2.4.11 Analytical Data

1-Benzyl-4-phenyl-1*H*-1,2,3-triazole (3a) [48]

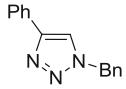

White solid; ^{1}H NMR (500 MHz, $CDCl_3$) δ 7.77−7.75 (m, 2H), 7.64 (s, 1H), 7.36−7.30 (m, 5H), 7.28−7.22 (m, 3H), 5.49 (s, 2H); ^{13}C NMR (125 MHz,

$CDCl_3$) δ 148.0, 134.6, 130.4, 128.9, 128.6, 128.5, 128.0, 127.8, 125.5, 119.5, 54.0; HRMS (ESI positive) calcd for $C_{15}H_{13}N_3$ [M + Na]$^+$: 258.1002, found: 258.1001.

2-(1-Benzyl-1*H*-1,2,3-triazol-4-yl)pyridine (3b) [49]

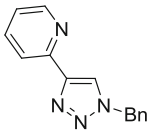

White solid; ^{1}H NMR (300 MHz, $CDCl_3$) δ 8.45−8.42 (m, 1H), 8.10−8.06 (m, 1H), 7.97 (s, 1H), 7.68−7.63 (m, 1H), 7.27−7.21 (m, 5H), 7.12−7.07 (m, 1H), 5.48 (s, 2H); ^{13}C NMR (75 MHz, $CDCl_3$) δ 150.0, 149.2, 148.5, 136.7, 134.2, 129.0, 128.6, 128.1, 122.7, 121.8, 120.0, 54.2; HRMS (ESI positive) calcd for $C_{14}H_{12}N_4$ [M + Na]$^+$: 259.0954, found: 259.0954.

1-Benzyl-4-(thiophen-3-yl)-1*H*-1,2,3-triazole (3c) [49]

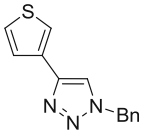

White solid; ^{1}H NMR (400 MHz, $CDCl_3$) δ 7.61-7.60 (m, 1H), 7.54 (s, 1H), 7.38-7.23 (m, 7H), 5.50 (s, 2H); ^{13}C NMR (100 MHz, $CDCl_3$) δ 144.2, 134.6, 131.7, 129.0, 128.6, 127.9, 126.2, 125.6, 120.9, 119.2, 54.0; HRMS (ESI positive) calcd for $C_{13}H_{11}N_3S$ [M + Na]$^+$: 264.0566, found: 264.0566.

1-Benzyl-4-pentyl-1*H*-1,2,3-triazole (3d) [50]

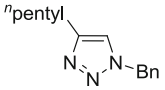

White solid; ^{1}H NMR (400 MHz, $CDCl_3$) δ 7.29-7.24 (m, 3H), 7.17-7.15 (m, 2H), 7.12 (s, 1H), 5.39 (s, 2H), 2.59 (t, J = 7.6 Hz, 2H), 1.57-1.53 (m, 2H), 1.24-1.21 (m, 4H), 0.79 (t, J = 7.2 Hz, 3H); ^{13}C NMR (100 MHz, $CDCl_3$) δ 148.7, 134.9, 128.8, 128.4, 127.7, 120.3, 53.7, 31.2, 28.9, 25.5, 22.2, 13.8; HRMS (ESI positive) calcd for $C_{14}H_{19}N_3$ [M + Na]$^+$: 252.1471, found: 252.1471.

1-Benzyl-4-cyclohexyl-1*H*-1,2,3-triazole (3e) [51]

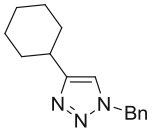

White solid; ^{1}H NMR (300 MHz, $CDCl_3$) δ 7.31-7.20 (m, 3H), 7.18-7.15 (m, 2H), 7.09 (s, 1H), 5.40 (s, 2H), 2.69-2.62 (m 1H), 1.95-1.94 (m, 2H), 1.71-1.60 (m, 3H), 1.37-1.10 (m, 5H); ^{13}C NMR (75 MHz, $CDCl_3$) δ154.0, 134.9, 128.8, 128.3,

127.8, 119.0, 53.7, 35.1, 32.8, 25.9, 25.8; HRMS (ESI positive) calcd for $C_{15}H_{19}N_3$ $[M + Na]^+$: 264.1471, found: 264.1471.

1-Benzyl-4-(tert-butyl)-1*H*-1,2,3-triazole (3f) [48]

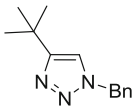

White solid; ^{1}H NMR (500 MHz, $CDCl_3$) δ 7.35-7.32 (m, 3H), 7.26-7.24 (m, 2H), 7.19 (s, 1H), 5.46 (s, 1H), 1.31 (s, 9H); ^{13}C NMR (125 MHz, $CDCl_3$) δ 157.9, 134.9, 128.8, 128.3, 127.8, 118.2, 53.6, 30.5, 30.1; HRMS (ESI positive) calcd for $C_{13}H_{17}N_3$ $[M + Na]^+$: 238.1315, found: 238.1314.

(1-Benzyl-1*H*-1,2,3-triazol-4-yl)methanol (3g) [51]

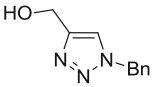

White solid; ^{1}H NMR (300 MHz, $CDCl_3$) δ 7.40 (s, 1H), 7.28-7.26 (m, 3H), 7.19-7.16 (m, 2H), 5.39 (s, 2H), 4.64 (d, J = 5.1 Hz, 2H), 4.20 (s, 1H); ^{13}C NMR (75 MHz, $CDCl_3$) δ 148.1, 134.4, 128.9, 128.5, 127.9, 121.7, 55.8, 53.9; HRMS (ESI positive) calcd for $C_{10}H_{11}N_3O$ $[M + Na]^+$: 212.0794, found: 212.0793.

1,4-Diphenyl-1*H*-1,2,3-triazole (3h) [48]

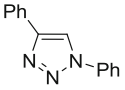

White solid; ^{1}H NMR (300 MHz, $CDCl_3$) δ 8.19 (s, 1H), 7.91 (d, J = 7.2 Hz, 2H), 7.79 (d, J = 7.8 Hz, 2H), 7.56-7.51 (m, 2H), 7.48-7.43 (m, 3H), 7.39-7.34 (m, 1H); ^{13}C NMR (75 MHz, $CDCl_3$) δ 148.3, 137.0, 130.2, 129.7, 128.8, 128.7, 128.3, 125.8, 120.4, 117.5; HRMS (ESI positive) calcd for $C_{14}H_{11}N_3$ $[M + Na]^+$: 244.0845, found: 244.0845.

1-Cinnamyl-4-phenyl-1*H*-1,2,3-triazole (3i) [52]

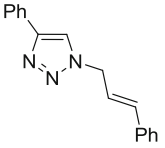

Light yellow solid; ^{1}H NMR (500 MHz, $CDCl_3$) δ 7.80 (d, J = 7.5 Hz, 2H), 7.76 (s, 1H), 7.38-7.35 (m, 4H), 7.33-7.21 (m, 4H), 6.30 (d, J = 16.0 Hz, 1H), 6.31 (dt, J = 16.0 Hz, 6.5 Hz, 1H), 5.09-5.08 (m, 2H); ^{13}C NMR (125 MHz, $CDCl_3$) δ 147.9, 135.3, 135.1, 130.5, 128.7, 128.6, 128.4, 128.0, 126.5, 125.5, 121.8, 119.3, 52.2; HRMS (ESI positive) calcd for $C_{17}H_{15}N_3$ $[M + Na]^+$: 284.1158, found: 284.1158.

Ethyl 2-(4-phenyl-1*H*-1,2,3-triazol-1-yl)acetate (3j) [51]

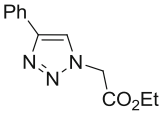

White solid; ^{1}H NMR (400 MHz, $CDCl_3$) δ 7.90 (s, 1H), 7.82 (d, J = 7.2 Hz, 2H), 7.40 (t, J = 7.6 Hz, 2H), 7.32 (t, J = 7.6 Hz, 1H), 5.17 (s, 2H), 4.24 (q, J = 7.2 Hz, 2H), 1.27 (t, J = 7.2 Hz, 3H); ^{13}C NMR (100 MHz, $CDCl_3$) δ 166.2, 148.0, 130.2, 128.7, 128.1, 125.6, 120.9, 62.3, 50.8, 13.9; HRMS (ESI positive) calcd for $C_{12}H_{13}N_3O_2$ [M + Na]$^+$: 254.0900, found: 254.0900.

***N*-Benzyl-1-(1-phenyl-1*H*-1,2,3-triazol-4-yl)methanamine (3k)**

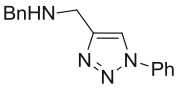

Brown solid; ^{1}H NMR (300 MHz, $CDCl_3$) δ 7.66-7.62 (m, 2H), 7.46-7.39 (m, 2H), 7.37-7.16 (m, 6H), 3.93 (s, 2H), 3.81 (s, 2H), 1.86 (s, 1H); ^{13}C NMR (75 MHz, $CDCl_3$) δ 147.4, 137.0, 129.5, 128.4, 128.3, 128.1, 126.9, 124.6, 120.3, 119.8, 53.2, 43.9; HRMS (ESI positive) calcd for $C_{16}H_{16}N_4$ [M + Na]$^+$: 287.1267, found: 287.1266.

4-Methyl-*N*-((1-phenyl-1*H*-1,2,3-triazol-4-yl)methyl)benzenesulfonamide (3l)

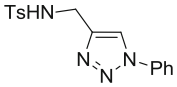

Yellow solid; ^{1}H NMR (400 MHz, $CDCl_3$) δ 7.80 (s, 1H), 7.73 (d, J = 8.4 Hz, 2H), 7.62-7.59 (m, 2H), 7.50-7.47 (m, 2H), 7.44-7.40 (m, 1H), 7.26-7.23 (m, 2H), 5.72 (s, 1H), 4.35 (d, J = 6.0 Hz, 2H), 2.34 (s, 3H); ^{13}C NMR (100 MHz, $CDCl_3$) δ 144.4, 143.6, 136.7, 129.7, 129.6, 128.8, 127.1, 124.8, 120.5, 120.3, 38.6, 21.3; HRMS (ESI positive) calcd for $C_{16}H_{16}N_4O_2S$ [M + Na]$^+$: 351.0886, found: 351.0885.

N,N-diisopropyl-2-phenyl-N′-tosylacetimidamide

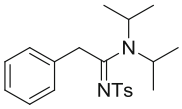

White solid; ^{1}H NMR (300 MHz $CDCl_3$) δ 7.85 (d, J = 8.1 Hz, 2H), 7.32-7.20 (m, 7H), 4.42 (s, 2H), 4.06-3.97 (m, 1H), 3.51-3.42 (m, 1H), 2.40 (s, 3H), 1.41 (d, J = 6.6 Hz, 6H), 0.88 (d, J = 6.6 Hz, 6H); ^{13}C NMR (75 MHz, $CDCl_3$) δ 163.3, 141.4, 141.4, 134.8, 128.9, 128.6, 127.8, 126.6, 126.0, 50.3, 47.9, 38.5, 21.3, 19.6, 19.6; HRMS (ESI positive) calcd for $C_{21}H_{28}N_2O_2S$ [M + Na]+: 395.1764, found: 395.1764.

2-cyclohexyl-N,N-diisopropyl-N′-tosylacetimidamide

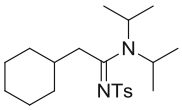

White solid; ^{1}H NMR (300 MHz $CDCl_3$) δ 7.81 (d, J = 8.4 Hz, 2H), 7.25 (d, J = 8.4 Hz, 2H), 4.17-4.09 (m, 1H), 3.54-3.45 (m, 1H), 2.94 (d, J = 7.2 Hz, 2H), 2.40 (s, 3H), 1.77-1.67 (m, 6H), 1.31-1.28 (m, 7H), 1.23-1.21 (m, 10H); ^{13}C NMR (75 MHz, $CDCl_3$) δ 164.7, 142.0, 141.1, 128.8, 125.9, 50.2, 47.8, 38.6, 37.1, 32.5, 26.4, 25.9, 21.3, 20.5, 20.1; HRMS (ESI positive) calcd for $C_{21}H_{34}N_2O_2S$ [M + Na]+: 401.2233, found: 401.2233.

N,N-diallyl-2-phenyl-N'-tosylacetimidamide

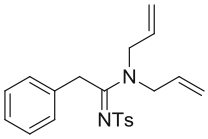

Yellow liquid; ^{1}H NMR (300 MHz $CDCl_3$) δ 7.80 (d, J = 8.1 Hz, 2H), 7.30-7.14 (m, 7H), 5.85-5.72 (m, 1H), 5.54-5.41 (m, 1H), 5.14 (dd, J = 10.2 Hz, 17.1 Hz, 4H), 4.42 (s, 2H), 4.11 (d, J = 6.3 Hz, 2H), 3.77 (d, J = 4.8 Hz, 2H), 2.38 (s, 3H); ^{13}C NMR (75 MHz, $CDCl_3$) δ 165.6, 141.7, 140.9, 133.9, 131.2, 131.1, 128.9, 128.8, 127.8, 126.7, 126.1, 118.4, 118.0, 50.6, 50.1, 36.5, 21.2; HRMS (ESI positive) calcd for $C_{21}H_{24}N_2O_2S$ [M + Na]+: 391.1451, found: 391.1451.

2.4.12 ^{1}H and ^{13}C NMR Spectra

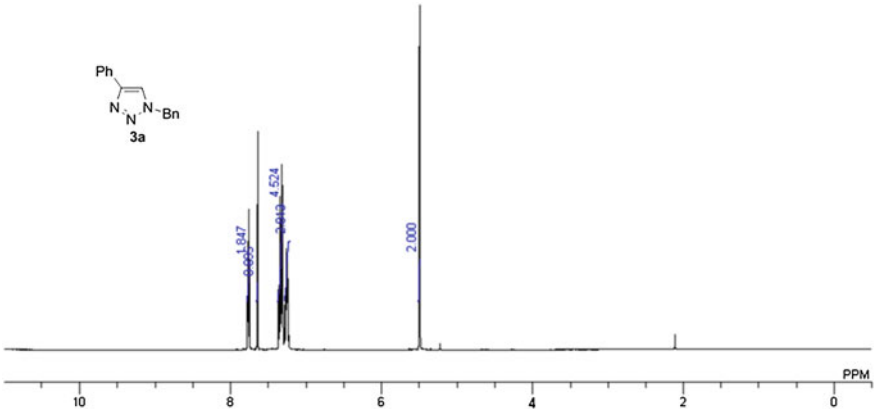

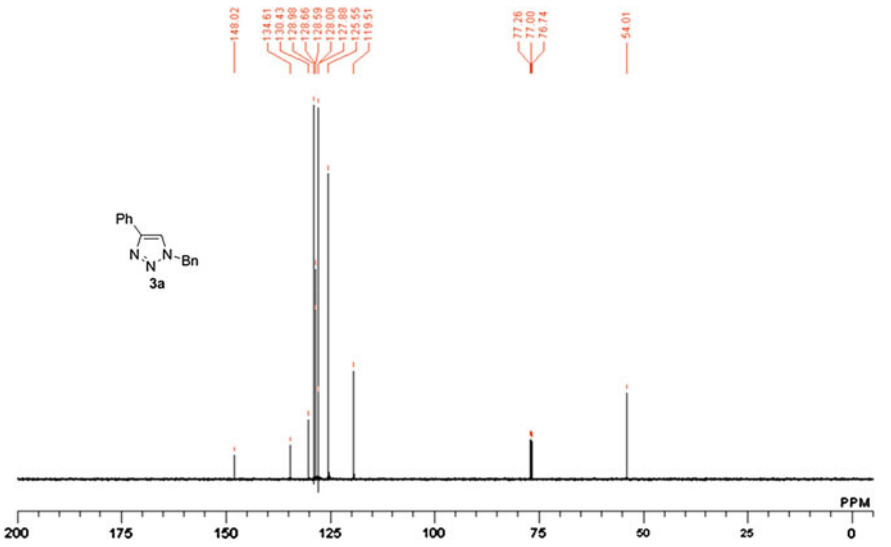
148.02
134.61
130.13
128.98
128.86
128.59
128.00
127.88
125.55
119.51
77.26
77.00
76.74
54.01
Ph
N
N
N
Bn
3a
PPM
200
175
150
125
100
75
50
25
0

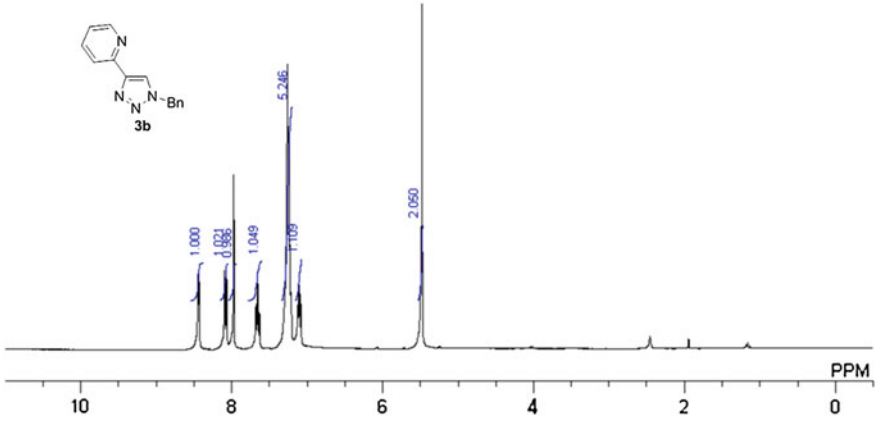
N
N
N
Bn
3b
5.246
1.000
1.021
0.936
1.049
7.109
2.050
PPM
10
8
6
4
2
0

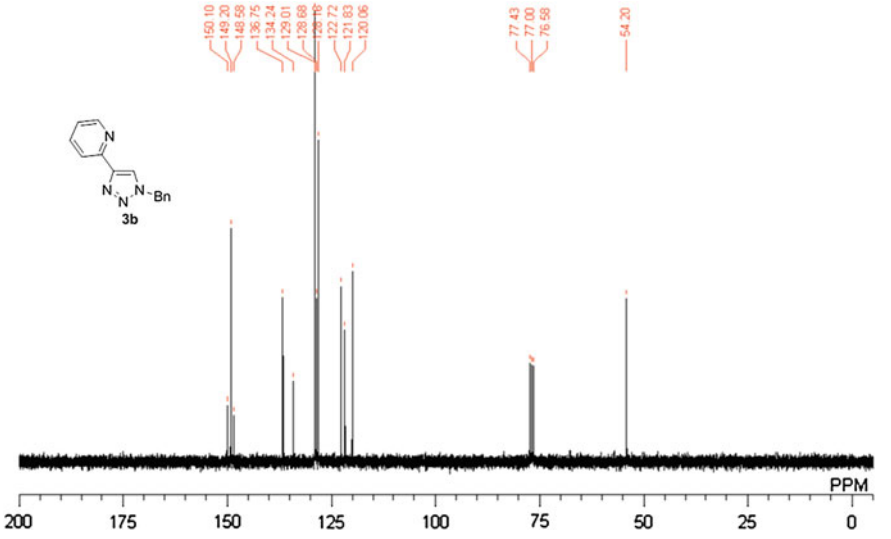
150.10
149.20
148.58
136.75
134.24
129.01
128.68
128.18
122.72
121.83
120.06
77.43
77.00
76.58
54.20
N
N
N
N
Bn
3b
PPM
200
175
150
125
100
75
50
25
0

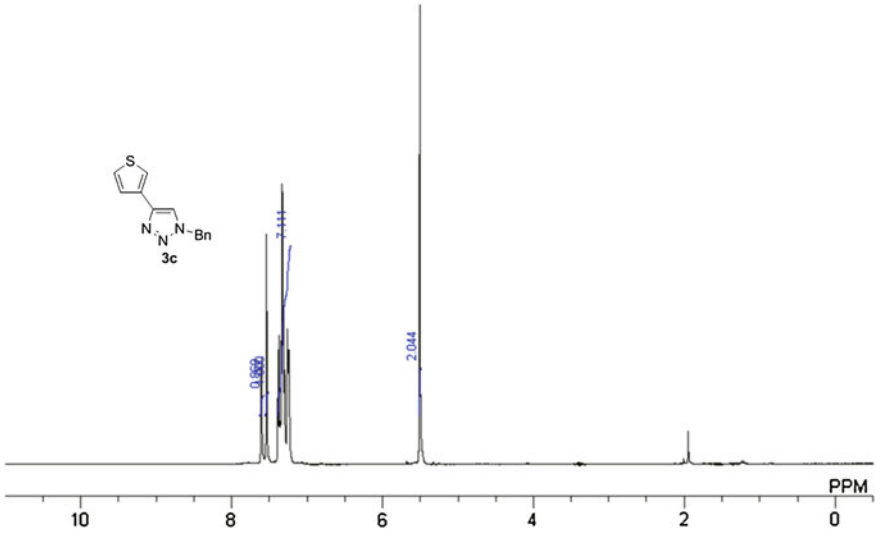
S
N
N
N
Bn
3c
7.111
2.044
0.869
PPM
10
8
6
4
2
0

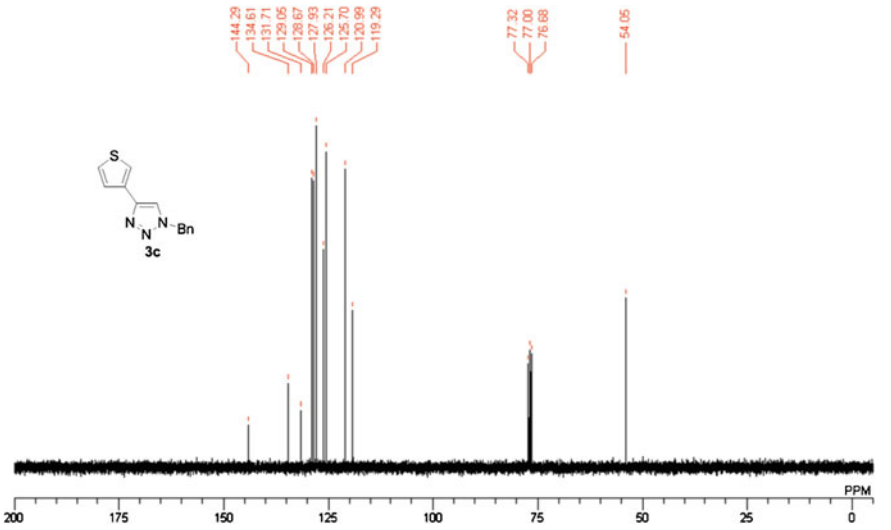
144.29
134.61
131.71
129.05
128.67
127.93
126.21
125.70
120.99
119.29
77.32
77.00
76.68
54.05
S
N
N
N
Bn
3c
PPM
200
175
150
125
100
75
50
25
0

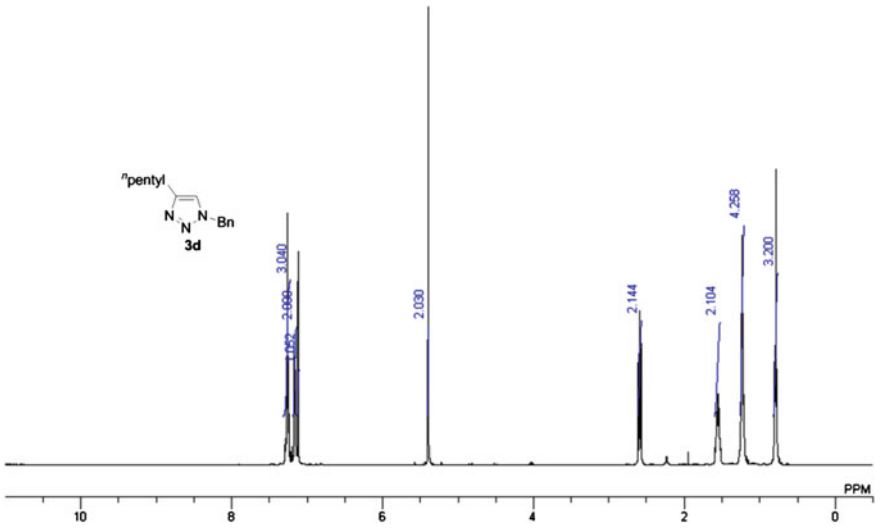
nentyl
N
N
N
Bn
3d
3.040
2.088
2.062
2.030
2.144
2.104
4.258
3.200
PPM
10
8
6
4
2
0

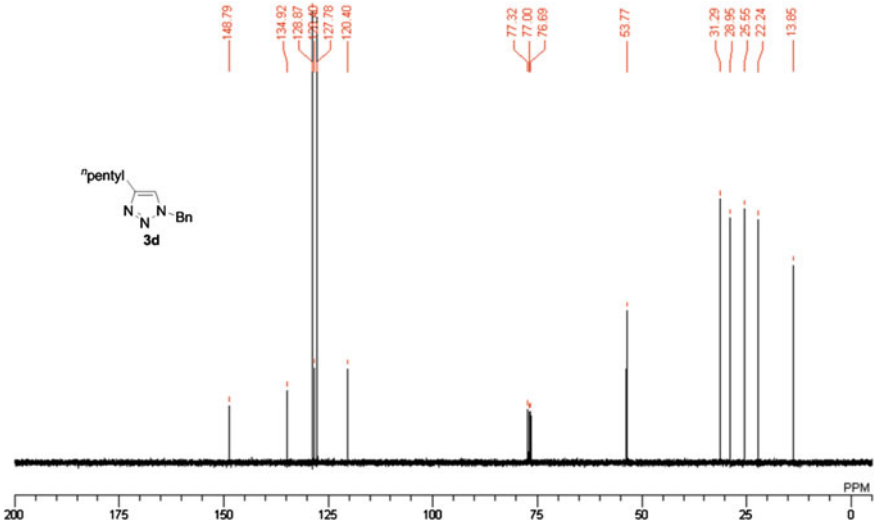
148.79
134.92
128.87
128.40
127.78
120.40
77.32
77.00
76.69
53.77
31.29
28.95
25.55
22.24
13.85
npentyl
N
N
N
Bn
3d
PPM
200
175
150
125
100
75
50
25
0

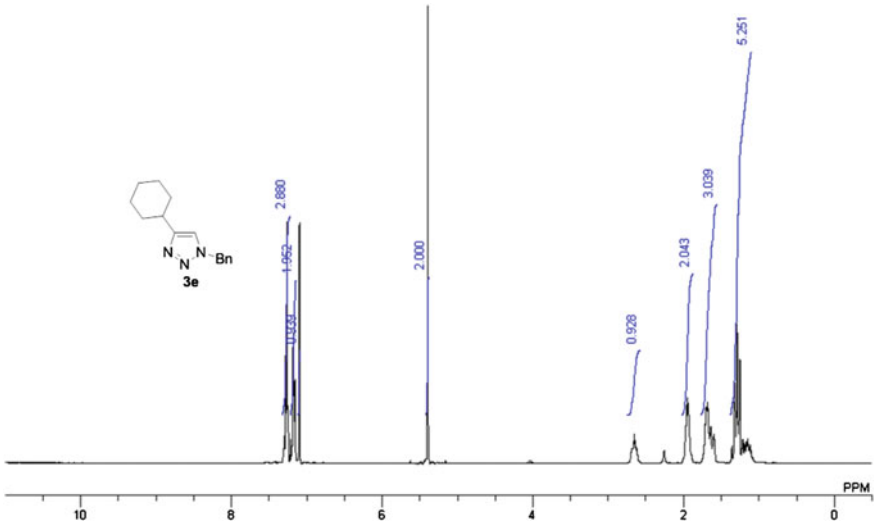
2.880
1.952
1.038
2.000
0.928
2.043
3.039
5.251
N
N
N
Bn
3e
PPM
10
8
6
4
2
0

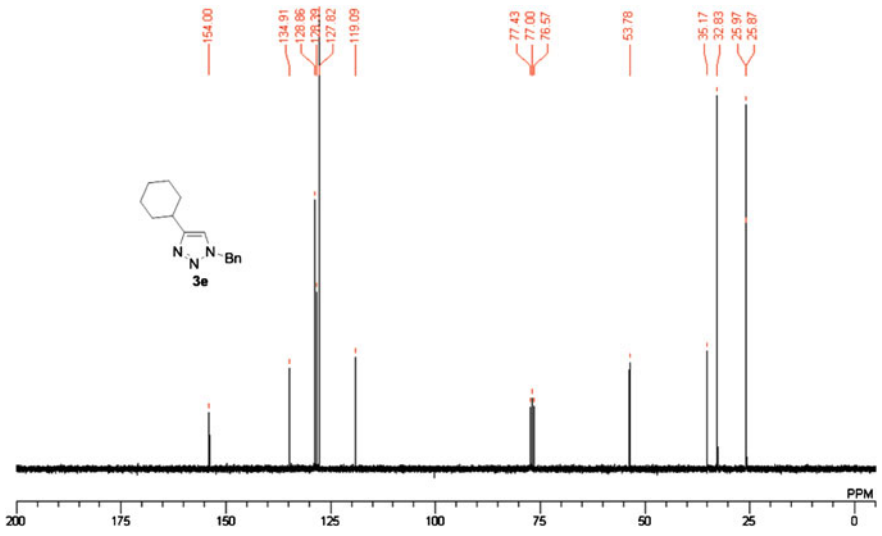
154.00
134.91
128.86
128.33
127.82
119.09
77.43
77.00
76.57
53.78
35.17
32.83
25.97
25.87
N
N
N
Bn
3e
PPM
200
175
150
125
100
75
50
25
0

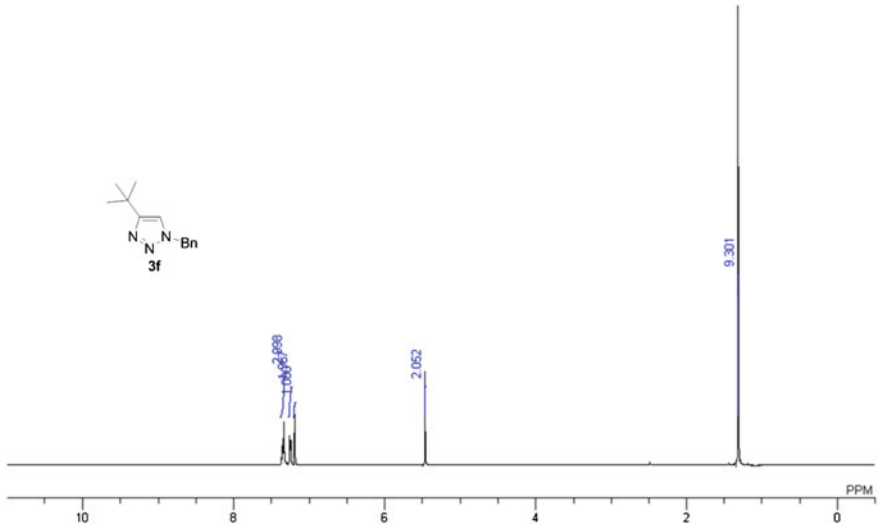
N
N
N
Bn
3f
9.301
2.052
PPM
10
8
6
4
2
0

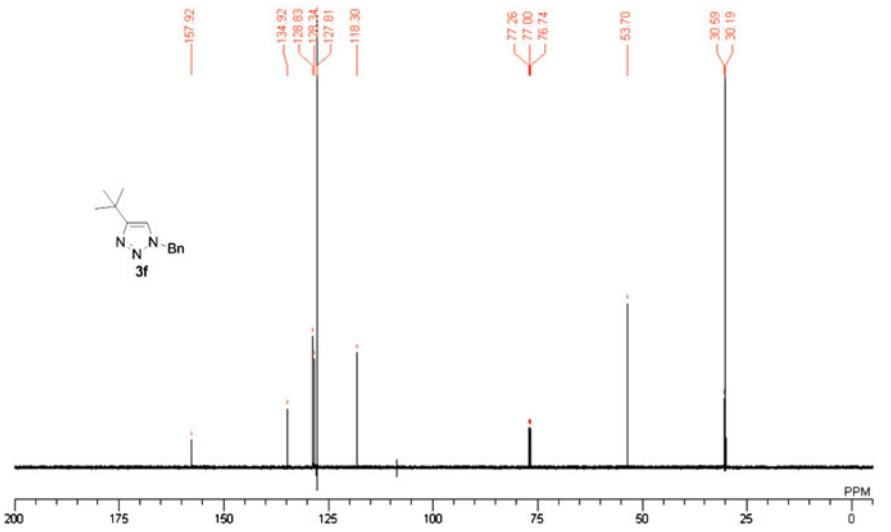
157.92
134.92
128.83
128.34
127.81
118.30
77.26
77.00
76.74
53.70
30.59
30.19
N
N
N
Bn
3f
PPM
200
175
150
125
100
75
50
25
0

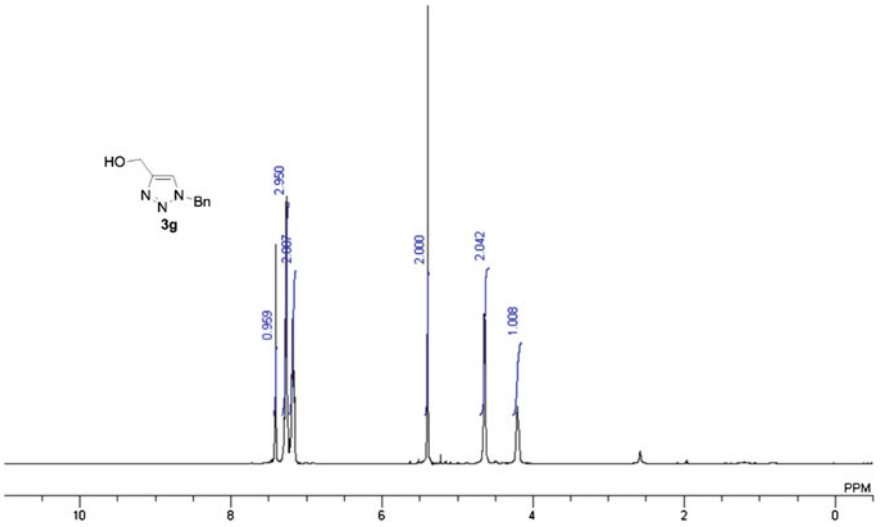
HO
N
N
N
Bn
3g
2.950
2.087
0.969
2.000
2.042
1.008
PPM
10
8
6
4
2
0

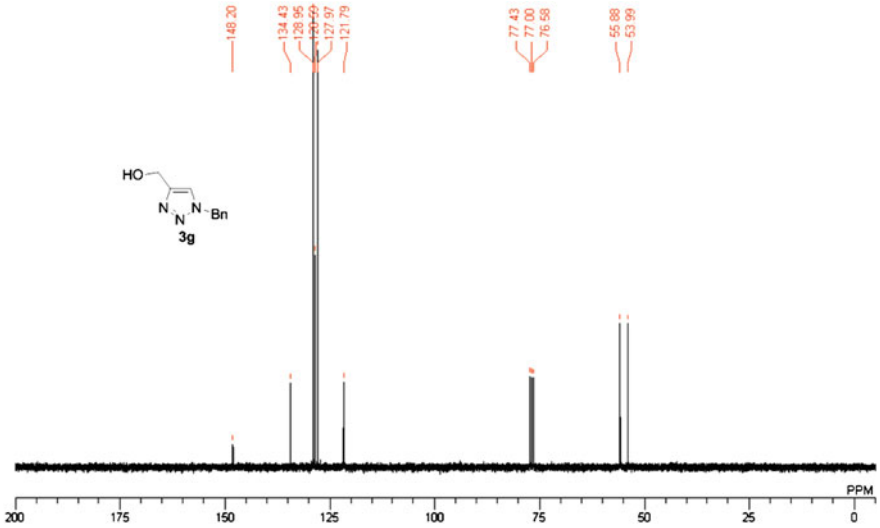
148.20
134.43
128.95
128.69
127.97
121.79
77.43
77.00
76.58
55.88
53.99
HO
N
N
N
Bn
3g
PPM
200
175
150
125
100
75
50
25
0

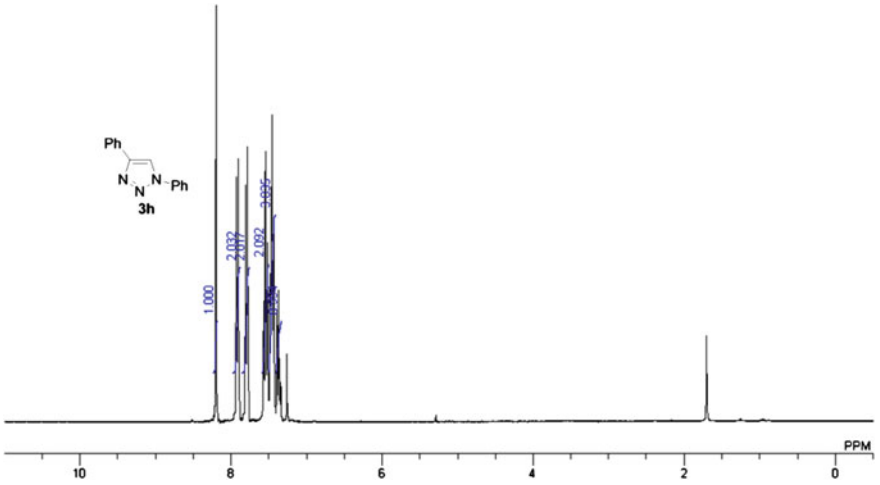
Ph
N
N
N
Ph
3h
1.000
2.032
2.017
2.092
3.035
PPM
10
8
6
4
2
0

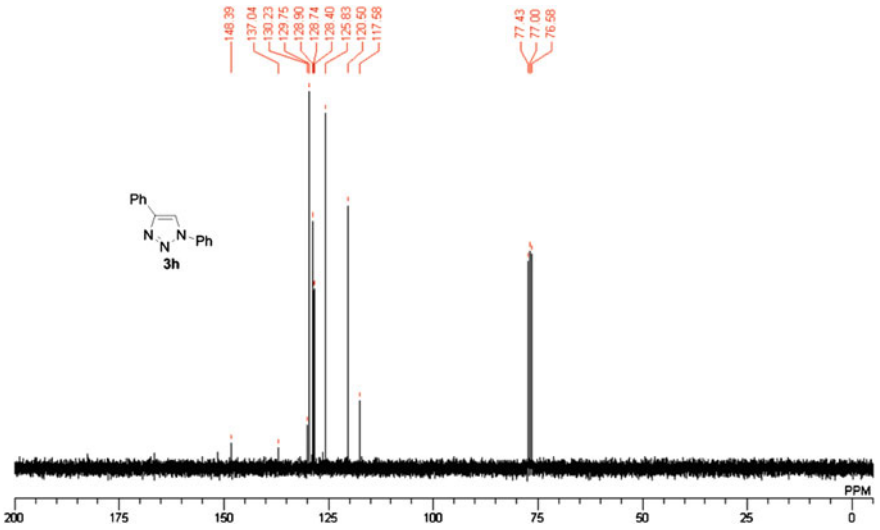
148.39
137.04
130.23
129.75
128.90
128.74
128.40
125.83
120.50
117.58
77.43
77.00
76.58
Ph
N
N
N
Ph
3h
PPM
200
175
150
125
100
75
50
25
0

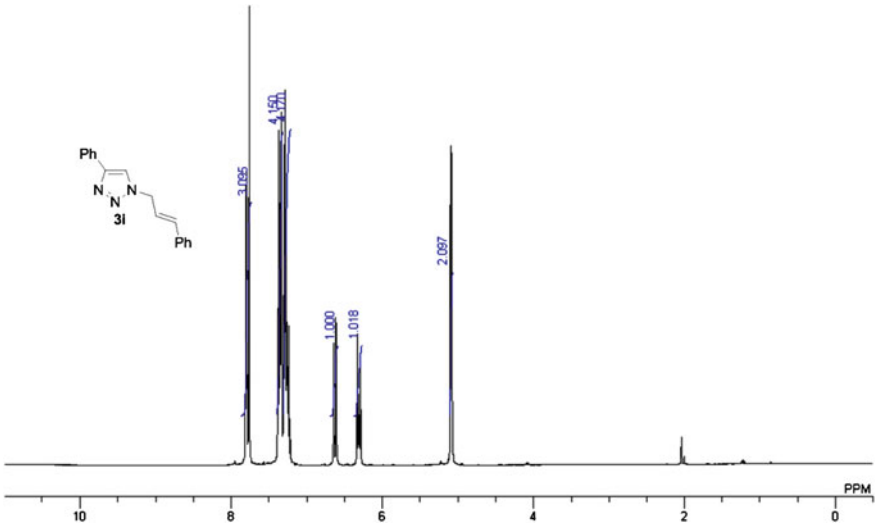
Ph
N
N
N
3l
Ph
3.095
4.150
4.171
1.000
1.018
2.097
PPM
10
8
6
4
2
0

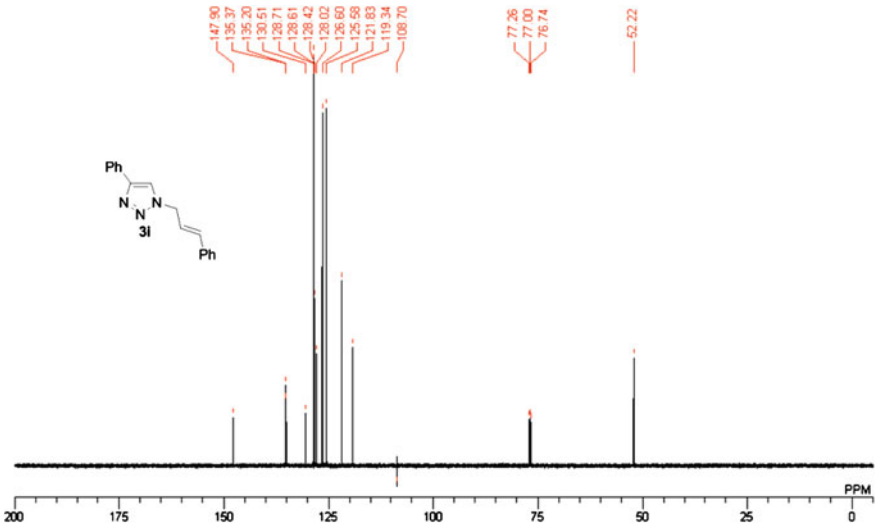
147.90
135.37
135.20
130.51
128.71
128.61
128.42
128.02
126.60
125.58
121.83
119.34
108.70
77.26
77.00
76.74
52.22
Ph
N
N
N
3l
Ph
PPM
200
175
150
125
100
75
50
25
0

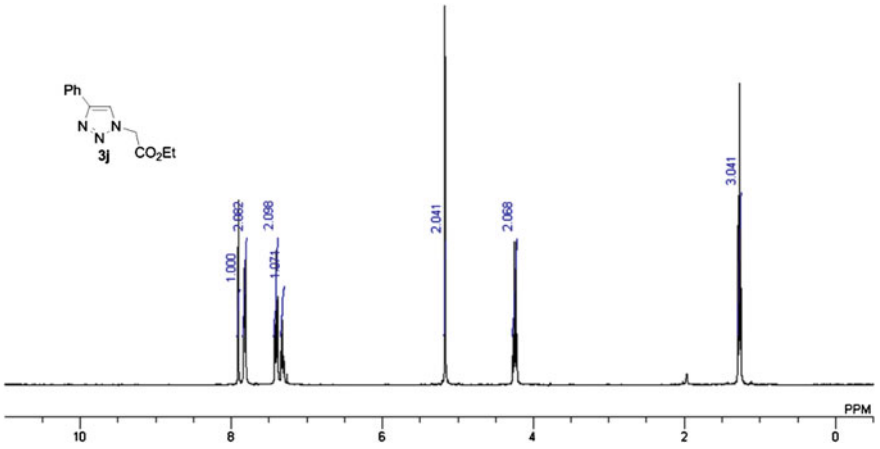
Ph
N
N
N
3j
CO2Et
1.000
2.662
2.098
1.071
2.041
2.068
3.041
PPM
10
8
6
4
2
0

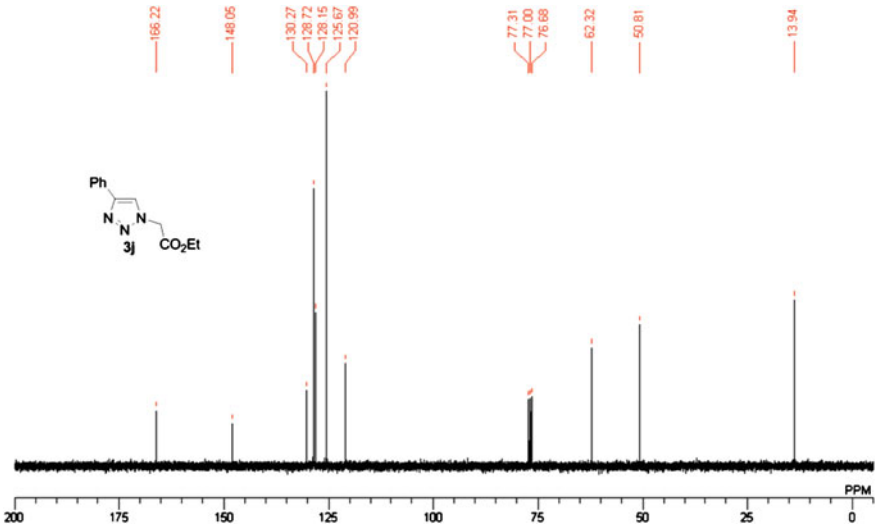
166.22
148.05
130.27
128.72
128.15
125.67
120.99
77.31
77.00
76.68
62.32
50.81
13.94
Ph
N
N
N
3j
CO2Et
PPM
200
175
150
125
100
75
50
25
0

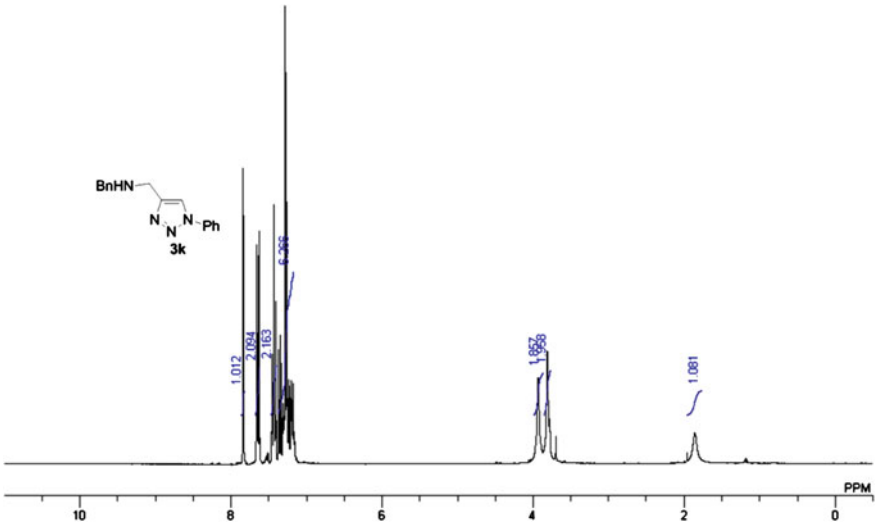
BnHN
N
N
N
Ph
3k
1.012
2.094
2.163
6.266
1.957
1.969
1.081
PPM
10
8
6
4
2
0

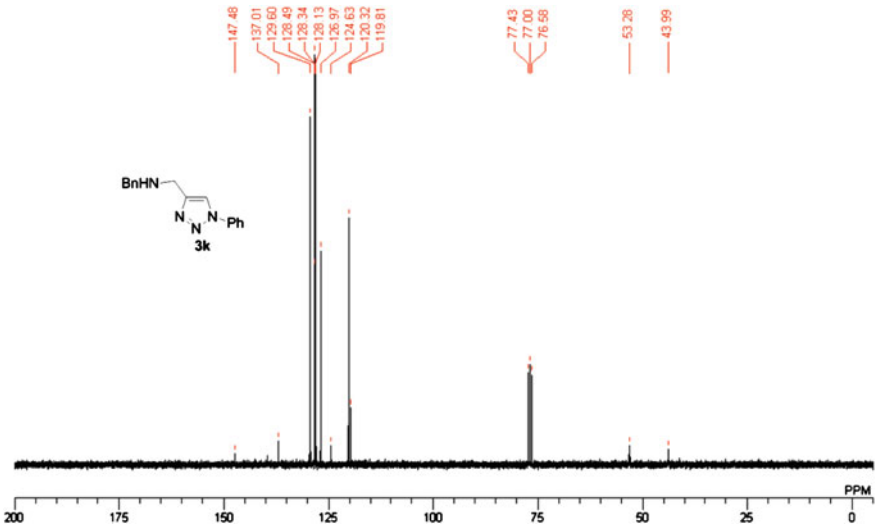
147.46
137.01
129.60
128.49
128.34
128.13
126.97
124.63
120.32
119.81
77.43
77.00
76.58
53.28
43.99
BnHN
N
N
N
Ph
3k
PPM
200
175
150
125
100
75
50
25
0

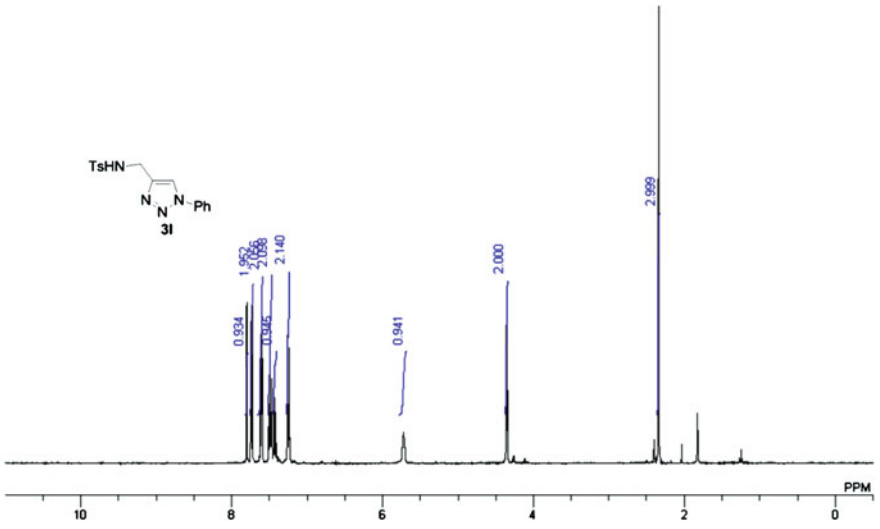
TsHN
N
N
N
Ph
3l
1.962
2.066
2.088
2.140
0.934
0.345
0.941
2.000
2.999
PPM
10
8
6
4
2
0

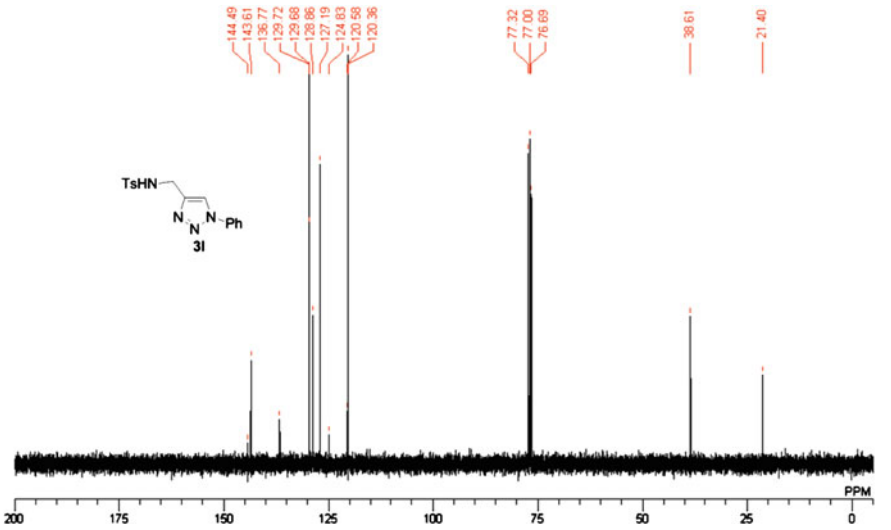
144.49
143.61
136.77
129.72
129.68
128.86
127.19
124.83
120.58
120.36
77.32
77.00
76.69
38.61
21.40
TsHN
N
N
N
Ph
3l
PPM
200
175
150
125
100
75
50
25
0

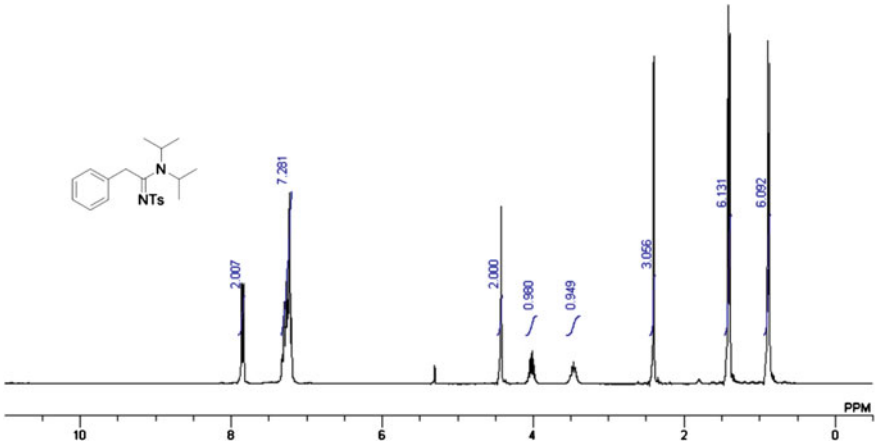
N
NTs
7.281
2.007
2.000
0.980
0.949
3.056
6.131
6.092
PPM
10
8
6
4
2
0

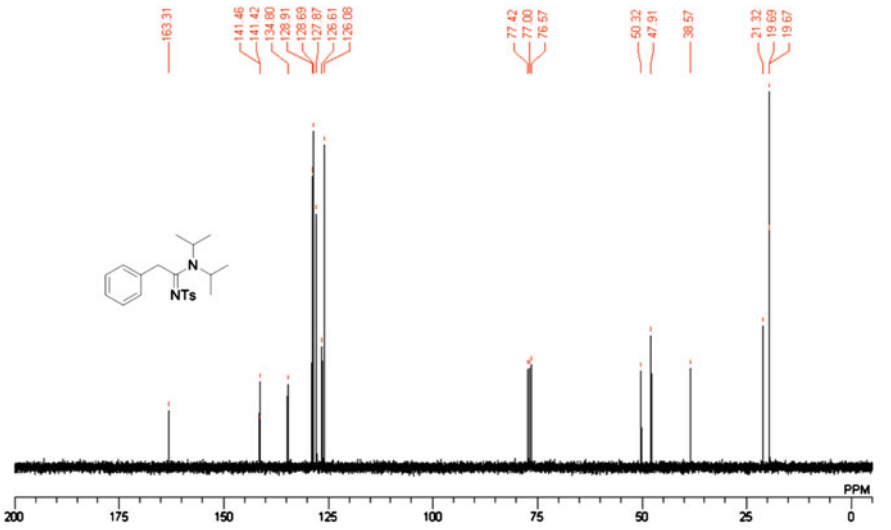
163.31
141.46
141.42
134.80
128.91
128.69
127.87
126.61
126.08
77.42
77.00
76.57
50.32
47.91
38.57
21.32
19.69
19.67
N
NTs
PPM
200
175
150
125
100
75
50
25
0

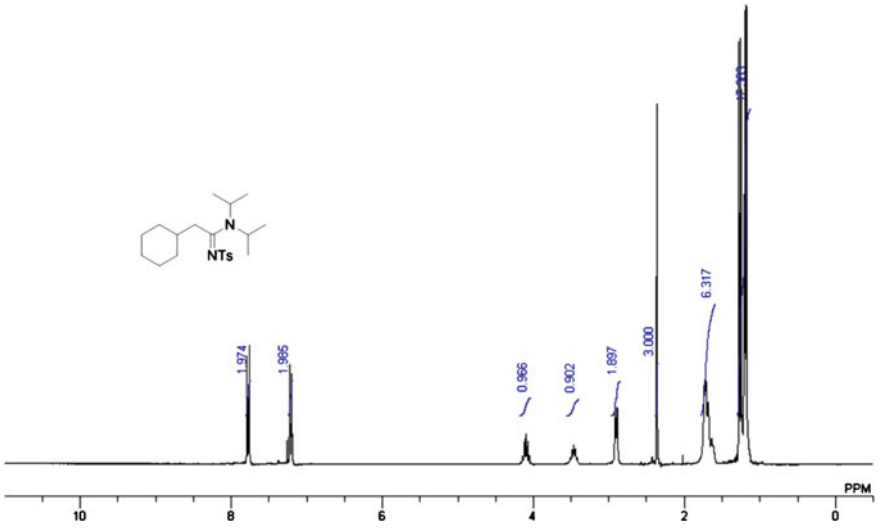
N
NTs
1.974
1.985
0.966
0.902
1.897
3.000
6.317
PPM
10
8
6
4
2
0

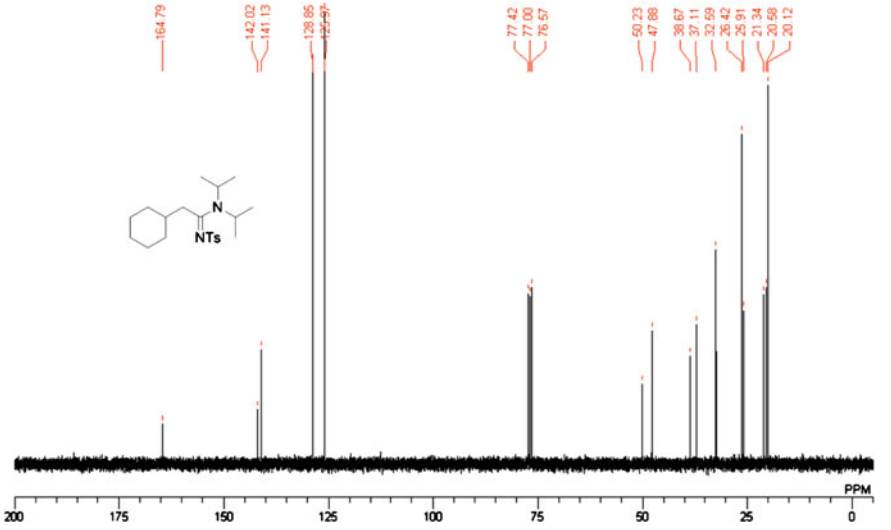
164.79
142.02
141.13
128.85
127.97
77.42
77.00
76.57
50.23
47.88
38.67
37.11
32.59
26.42
25.91
21.34
20.58
20.12
N
NTs
PPM
200
175
150
125
100
75
50
25
0

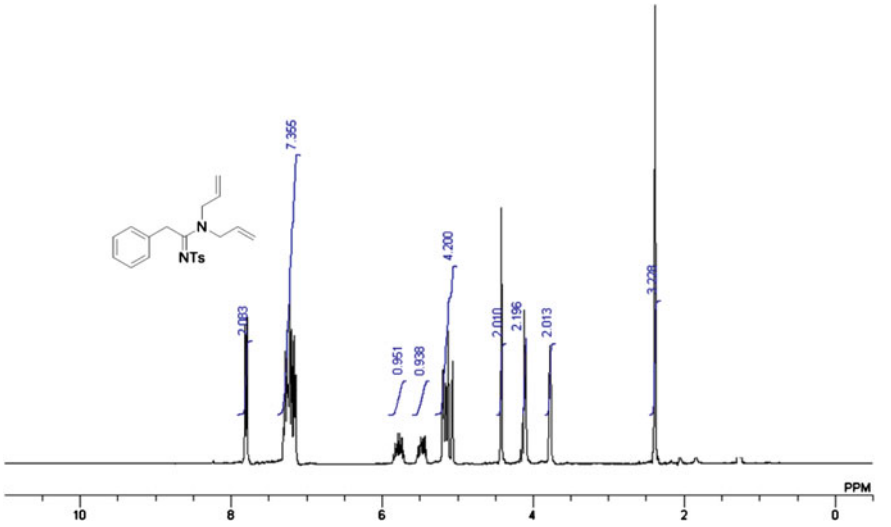
7.365
4.200
3.228
3.003
2.010
2.196
2.013
0.951
0.938
N
NTs
PPM
10
8
6
4
2
0

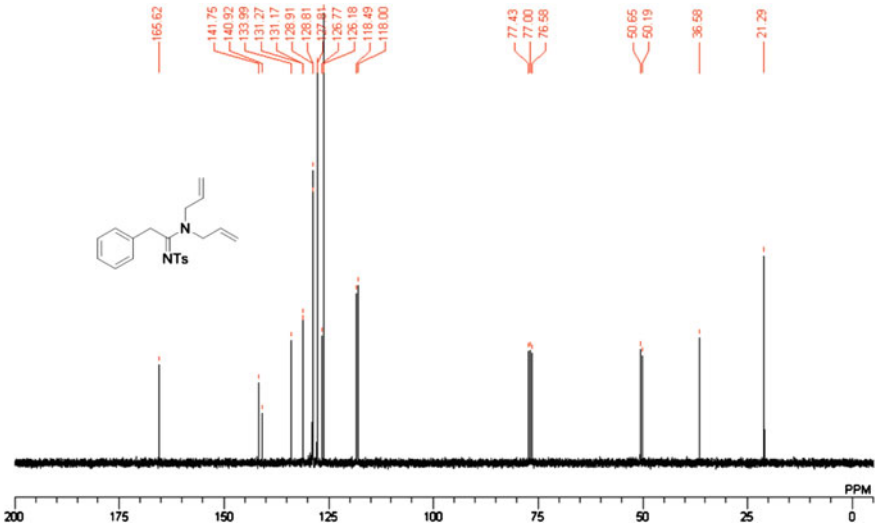

References

1. Zielasek V, Jürgens B, Schulz C et al (2006) Gold catalysts: nanoporous gold foams. Angew Chem Int Ed 45:8241–8244
2. Xu C, Su J, Xu X et al (2007) Low temperature CO oxidation over unsupported nanoporous gold. J Am Chem Soc 129:42–43
3. Xu C, Xu X, Su J et al (2007) Research on unsupported nanoporous gold catalyst for CO oxidation. J Catal 252:243–248
4. Wittstock A, Neumann B, Schaefer A et al (2009) Nanoporous Au: an unsupported pure gold catalyst? J Phys Chem C 113:5593–5600
5. Yin H, Zhou C, Xu C et al (2008) Aerobic oxidation of d-Glucose on support-free nanoporous gold. J Phys Chem C 112:9673–9678
6. Wittstock A, Zielasek V, Biener J et al (2010) Nanoporous gold catalysts for selective gas-phase oxidative coupling of methanol at low temperature. Science 327:319–322
7. Zhang J, Liu P, Ma H et al (2007) Nanostructured porous gold for methanol electro-oxidation. J Phys Chem C 111:10382–10388
8. Yu C, Jia F, Ai Z et al (2007) Direct oxidation of methanol on self-supported nanoporous gold film electrodes with high catalytic activity and stability. Chem Mater 19:6065–6067
9. Zeis R, Lei T, Sieradzki K et al (2008) Catalytic reduction of oxygen and hydrogen peroxide by nanoporous gold. J Catal 253:132–138
10. Biener J, Nyce GW, Hodge AM et al (2008) Nanoporous plasmonic metamaterials. Adv Mater 20:1211–1217
11. Bonroy K, Friedt JM, Frederix F et al (2004) A comparative plasmonic study of nanoporous and evaporated gold films. Anal Chem 76:4299–4306
12. Hieda M, Garcia R, Dixon M et al (2004) Ultrasensitive quartz crystal microbalance with porous gold electrodes. Appl Phys Lett 84:628–630
13. Kramer D, Viswanath RN, Wiessmueller J et al (2004) Surface-stress induced macroscopic bending of nanoporous gold cantilevers. Nano Lett 4:793–796
14. Biener J, Wittstock A, Zepeda-Ruiz LA et al (2009) Surface-chemistry-driven actuation in nanoporous gold. Nat Mater 8:47–51

15. Asao N, Ishikawa Y, Hatakeyama N et al (2010) Nanostructured materials as catalysts: nanoporous-gold-catalyzed oxidation of organosilanes with water. Angew Chem Int Ed 49:10093–10095
16. Anaka S, Kaneko T, Asao N et al (2011) A nanostructured skeleton catalyst: Suzuki-coupling with a reusable and sustainable nanoporous metallic glass Pd-catalyst. Chem Commun 47:5985–5987
17. Rostovtsev VV, Green LG, Fokin VV et al (2002) Stepwise Huisgen cycloaddition process: copper(I)-catalyzed regioselective "Ligation" of azides and terminal alkynes. Angew Chem Int Ed 41:2596–2599
18. Tornøe CW, Christensen C, Meldal M (2002) Peptidotriazoles on solid phase: [1,2,3]-triazoles by regiospecific copper(I)-catalyzed 1,3-dipolar cycloadditions of terminal alkynes to azides. J Org Chem 67:3057–3062
19. Tron GC, Pirali T, Billington RA et al (2008) Regioselective intramolecular dipolar cycloaddition of azides and unsymmetrical alkynes. Med Res Rev 28:278–308
20. Melda M, Tornøe CW (2008) Cu-catalyzed azide-alkyne cycloaddition. Chem Rev 108:2952–3015
21. Amblard F, Cho JH, Schinazi RF (2009) Cu(I)-catalyzed Huisgen azide−alkyne 1,3-dipolar cycloaddition reaction in nucleoside, nucleotide, and oligonucleotide chemistry. Chem Rev 109:4207–4220
22. Pachon LD, van Maarseven JH, Rothenberg G (2005) Click chemistry: copper clusters catalyse the cycloaddition of azides with terminal alkynes. Adv Synth Catal 347:811–815
23. Molteni G, Bianchi CL, Marinoni G et al (2006) Cu/Cu-oxide nanoparticles as catalyst in the "click" azide–alkyne cycloaddition. New J Chem 30:1137–1139
24. Lipshutz BH, Taft BR (2006) Terogeneous copper-in-charcoal-catalyzed click chemistry. Angew Chem Int Ed 45:8235–8238
25. Chassaing S, Kumarraja M, Sani Souna Sido A et al (2007) Click chemistry in cuI-zeolites: the Huisgen [3 + 2]-cycloaddition. Org Lett 9:883–886
26. Chassaing S, Sani Souna Sido A, Alix A et al (2008) "Click chemistry" in zeolites: copper(I) zeolites as new heterogeneous and ligand-free catalysts for the Huisgen [3+2] cycloaddition. Chem Eur J 14:6713–6721
27. Alix A, Chassaing S, Pale P et al (2008) 'Click chemistry' in cuI-zeolites: a convenient access to glycoconjugates. Tetrahedron 64:8922–8929
28. Miao T, Wang L (2008) Regioselective synthesis of 1,2,3-triazoles by use of a silica-supported copper(I) catalyst. Synthesis 2008:363–368
29. Sharghi H, Khalifeh R, Mahdi Doroodmand M (2009) Copper nanoparticles on charcoal for multicomponent catalytic synthesis of 1,2,3-triazole derivatives from benzyl halides or alkyl halides, terminal alkynes and sodium azide in water as a "green" solvent. Adv Synth Catal 351:207–218
30. Lee BS, Yi M, Chu SY et al (2010) Copper nitride nanoparticles supported on a superparamagnetic mesoporous microsphere for toxic-free click chemistry. Chem Commun 46:3935–3937
31. Himo F, Lovell T, Hilgraf R et al (2005) Copper(I)-catalyzed synthesis of azoles. DFT study predicts unprecedented reactivity and intermediates. J Am Chem Soc 127:210–216
32. Hayes JR, Hodge AM, Biener J et al (2006) Monolithic nanoporous copper by dealloying Mn–Cu. J Mater Res 21:2611–2616
33. Qi Z, Zhao C, Wang X et al (2009) Formation and characterization of monolithic nanoporous copper by chemical dealloying of Al−Cu alloys. J Phys Chem C 113:6694–6698
34. Zhao C, Qi Z, Wang X et al (2009) Fabrication and characterization of monolithic nanoporous copper through chemical dealloying of Mg–Cu alloys. Corros Sci 51:2120–2125
35. Zhang Z, Wang Y, Qi Z et al (2009) Generalized fabrication of nanoporous metals (Au, Pd, Pt, Ag, and Cu) through chemical dealloying. J Phys Chem C 113:12629–12636
36. Chen LY, Yu JS, Fujita T et al (2009) Nanoporous copper with tunable nanoporosity for SERS applications. Adv Funct Mater 19:1221–1226

37. Mellor JR, Coville NJ, Sofianos AC et al (1997) Raney copper catalysts for the water-gas shift reaction:I. preparation, activity and stability. Appl Catal A 164:171–183
38. Mellor JR, Coville NJ, Durbach SH et al (1998) Acid leached Raney copper catalysts for the water–gas shift reaction. Appl Catal A 171:273–281
39. Liu WB, Zhao S, Li N et al (2010) Microstructure evolution of monolithic nanoporous copper from dual-phase Al 35 atom % Cu alloy. J Electrochem Soc 157:D666–D670
40. Liu WB, Zhang SC, Li N et al (2011) Influence of phase constituent and proportion in initial Al–Cu alloys on formation of monolithic nanoporous copper through chemical dealloying in an alkaline solution. Corros Sci 53:809–814
41. Bae I, Han H, Chang S (2005) Highly efficient one-pot synthesis of N-sulfonylamidines by Cu-catalyzed three-component coupling of sulfonyl azide, alkyne, and amine. J Am Chem Soc 127:2038–2039
42. Moulder JF, Stickle WF, Sobol PE et al (1995) Handbook of X ray photoelectron spectroscopy: a reference book of standard spectra for identification and interpretation of XPS data. Physical Electronics, Minnesota
43. Ahlquist M, Fokin VV (2007) Enhanced reactivity of dinuclear copper(I) acetylides in dipolar cycloadditions. Organometallics 26:4389–4391
44. Hein JE, Fokin VV (2010) Copper-catalyzed azide–alkyne cycloaddition (CuAAC) and beyond: new reactivity of copper(I) acetylides. Chem Soc Rev 39:1302–1315
45. Straub BF (2007) m-Acetylide and m-alkenylidene ligands in ''click'' triazole syntheses. Chem Commun 3868–3870
46. Zhou Y, Lecourt T, Micouin L (2010) Direct synthesis of 1,4-disubstituted-5-alumino-1,2,3-triazoles: copper-catalyzed cycloaddition of organic azides and mixed aluminum acetylides. Angew Chem Int Ed 49:2607–2610
47. Wang D, Li N, Zhao M et al (2010) Solvent-free synthesis of 1,4-disubstituted 1,2,3-triazoles using a low amount of $Cu(PPh_3)_2NO_3$ complex. Green Chem 12:2120–2123
48. Fletcher JT, Keeney ME, Walz SE (2010) 1-allyl- and 1-benzyl-3-methyl-1,2,3-triazolium salts via tandem click transformations. Synthesis 19:3339–3345
49. Alonso F, Moglie Y, Radivoy G (2010) Unsupported copper nanoparticles in the 1,3-dipolar cycloaddition of terminal alkynes and azides. Eur J Org Chem 10:1875–1884
50. Kamijo S, Jin T, Huo Z et al (2004) Highly N_2-selective palladium-catalyzed arylation of 1,2,3-triazoles. J Org Chem 69:2386–2393
51. Qian LH, Yan XQ, Fujita T et al (2007) Surface enhanced Raman scattering of nanoporous gold: smaller pore sizes stronger enhancements. Appl Phys Lett 90:153120–153123
52. Mohanty A, Garg N, Jin R (2010) A universal approach to the synthesis of noble metal nanodendrites and their catalytic properties. Angew Chem Int Ed 49:4962–4966

http://www.springer.com/978-4-431-54930-7

Development of New Catalytic Performance of Nanoporous Metals for Organic Reactions

Yan, M.

2014, XVI, 123 p. 153 illus., 16 illus. in color., Hardcover
ISBN: 978-4-431-54930-7